1-1-1967

Radiation effects in zinc oxide:zinc under bombardment with KeV ions.

J. W. Lynden Hastings
University of Windsor

RADIATION EFFECTS IN ZnO:Zn UNDER BOMBARDMENT WITH KeV IONS

by
J. W. Lynden Hastings

A Thesis
Submitted to the Faculty of Graduate Studies Through the Department of Physics in Partial Fulfillment of the Requirements for the Degree of Doctor of Philosophy at the University of Windsor.

Windsor, Ontario
1967

Approved

N E Hedgecock

Dr. N. E. Hedgecock.

David Robinson

Dr. D. Robinson

A van Wijngaarden

Dr. A. van Wijngaarden
(Supervisor)

ABSTRACT

The energy loss, light output, depth of deterioration and the deterioration constant have been determined as a function of energy for various atomic projectiles impinging upon samples of a powdered ZnO:Zn phosphor at energies begow 105 KeV.

The energy loss was observed as a reduction in the light output when projectiles traversed thin regions of previously damaged phosphor. The energy losses for heavier projectiles (^{14}N, ^{40}Ar, ^{84}Kr), relative to hydrogen, were found to be lower than those predicted for an amorphous stopping medium.

The light output for a given projectile was found to be approximately proportional to the amount of energy lost in electronic collisions.

When a phosphor is subjected to prolonged bombardment by heavy ions the deterioration depth is fairly well defined and its value was determined by a measurement of the energy loss of a hydrogen beam in traversing the damaged region. The depths are very large, are proportional to the projectile velocity and seem to be determined to a significant degree by electronic stopping.

The deterioration constant, C, is a measure of the ability of a projectile to deteriorate a phosphor and its value is proportional to the number of defects introduced in unit distance along the trajectory of the projectile. The constant was determined from measurements of the efficiencies η, and η_o, of partly damaged and undamaged phosphor, respectively, using the observed relationship,

$$C = (\eta / \eta_o - 1) n^{-1}$$

where n is the irradiation dose. The relative magnitudes of the C values for ^{14}N and ^{40}Ar were found to be in agreement with measured nuclear energy loss cross sections for these projectiles.

ACKNOWLEDGEMENTS

I would like to express my appreciation to Dr. Arie van Wijngaarden for his assistance in my work and in the preparation of this dissertation.

TABLE OF CONTENTS

LIST OF FIGURES

LIST OF TABLES

CHAPTER I

INTRODUCTION

When phosphors are subjected to low energy (KeV) ion bombardment two effects may be readily observed. The first is the production of light under the ion excitation and the second, the reduction in the intensity of this light after prolonged bombardment as a result of radiation damage. The purpose of this dissertation is to determine the relationship between the energy loss mechanism and these two effects. The bulk of the experimental results are for a ZnO:Zn stopping medium and some observations were made with a ZnS:Ag phosphor.

A. The Energy Loss of Fast Atomic Particles

i. Energy Loss Mechanism - When an atomic projectile traverses a small distance, dR, of a stopping medium it loses a small amount of energy dE_e, in inelastic collisions with electrons and a small amount of energy dE_n, in elastic collisions with the target atoms. Thus the total stopping power of the medium equals the sum of the electronic and nuclear stopping powers;

(I. A. 1) $$- (dE / dR) = (-dE / dR)_e + (-dE / dR)_n .$$

The magnitude of dE / dR depends on the density of the stopping medium. One may, however, introduce the stopping cross section per target atom, which, to a first approximation, should be independent of the density. The total stopping cross section, S, which consists of electronic and nuclear components, S_e and S_n, respectively is given by

(I. A.) $$S = S_e + S_n$$

and is related to the stopping power by

(I. A. 3) $$- dE / dR = N S,$$

where N is the number of stopping atoms per unit volume.

For projectile velocities less than v_o, the velocity of an electron in the first Bohr orbit, the stopping cross sections have been studied by Lindhard and Scharff (1961) and Lindhard et al. (1963a+b). To faciliate the discussion of the cross sections, the variables

$$\rho = 4 \pi R N M_2 a^2 M_1 / (M_1 + M_2)^2$$

(I. A. 4) and

$$\epsilon = a M_2 E / Z_1 Z_2 e^2 (M_1 + M_2) ,$$

were introduced as dimensionless measures of range, R, and energy, E, respectively. The subscripts, 1 and 2, refer to the incident and target atoms, respectively. M, A, Z and e are the mass, mass number, atomic number and electronic charge, respectively. The screening parameter a is given by,

(I. A. 5) $$a = .8853 a_o (Z_1^{2/3} + Z_2^{2/3})^{-1/2}$$

where a_o is the radius of the first Bohr orbit in hydrogen.

Fig. 1, which is a reproduction of a curve presented by Lindhard et al. (1963), is a plot of the differential nuclear energy loss, $(d\epsilon / d\rho)_n$, versus $\epsilon^{1/2}$. The curve was derived by assuming a Thomas-Fermi potential between the colliding atoms and is discussed in A.I .

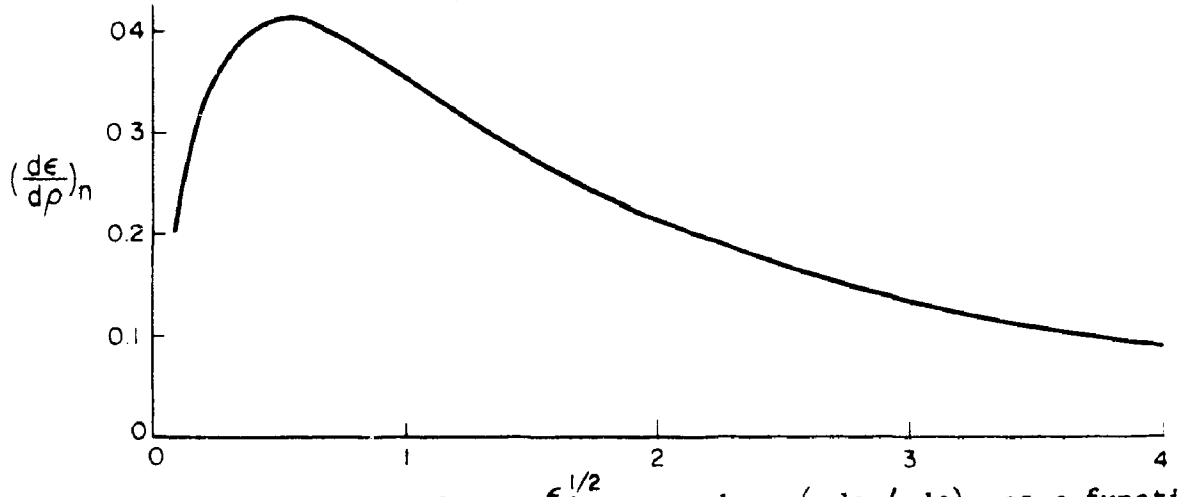

Fig. 1. The nuclear differential energy loss $(d\epsilon / d\rho)_n$ as a function of $\epsilon^{1/2}$ (from Lindhard et al. 1963a)

The shape of the nuclear energy loss curve may be qualitatively understood by assuming a screened coulomb potential;

(I.A.6) $$V(r) = \frac{Z_1 Z_2 e^{-r/a}}{r} ,$$

which yields approximately the same results as the more accurate Thomas-Fermi potential. For a pure coulomb potential, where the colliding atoms are stripped of all of their electrons, the distance of closest approach is given by

(I.A.7) $$b = \frac{2 Z_1 Z_2 e^2 (M_1 + M_2)}{M_1 M_2 v^2}$$

where v is the relative velocity. The distance of closest approach, b', in the screened coulomb field is given by,

(I.A.8) $$b = b' e^{b'/a} .$$

For low velocities $b' / a > 1$ and the scattering takes place in the screened coulomb field which falls off much more rapidly with r than does the coulomb field. For $b' >> a$ the collisions approach those of billiard balls, whose energy loss cross section is proportional to the energy, so that at low energies $(d\epsilon / d\rho)_n$ in the figure, increases quite rapidly with increasing values of $\epsilon^{1/2}$. At high velocities $b' << a$ and much of the significant scattering takes place with $r < a$, where the interaction potential is essentially coulombic and the stopping cross section has the well known (1 / E) ln E dependence, characteristic of Rutherford scattering, which decreases with increasing values of $\epsilon^{1/2}$. For $b' \simeq a$ the significant scattering takes place in an r^{-2} potential where the stopping cross section is a constant independent of the projectile energy.

The electronic energy loss mechanism is somewhat analogous to that of the nuclear energy loss. At high energy where the speed of the projectile is much larger than the orbital speed of the electrons in the stopping medium, the latter can be considered at rest and the energy loss mechanism is essentially of the Rutherford type, ie;

(I. A. 9) $$dE / dR = (4 \pi Z_1^2 e^4 / m v^2) N Z_2 L,$$

where m is the electron mass and

(I. A. 10) $$L = \ln (2 m v^2 / I).$$

L represents the logarithm of the ratio between the maximum and the minimum energy transfer. The maximum speed which may be imparted by a heavy projectile to an electron initially at rest, in a head on collision, is twice the projectile velocity. Thus the maximum energy transfer is $2 m v^2$. The average excitation energy, I, represents the minimum energy that must be transferred to excite electrons.

At low speeds the electrons in the target material can no longer be considered at rest and Eq. (I. A. 10) no longer holds. For velocities $v < v_o$ Lindhard and co-workers have studied L and found that it is proportional to v^3. Thus at low velocities dE / dR is proportional to v. The complete expression for the differential energy loss to electrons is given by,

(I. A. 11) $$(d\epsilon / d\rho)_e = K \epsilon^{1/2},$$

where

(I. A. 12) $$K = \frac{\xi_e \ .0793 \ Z_1^{1/2} \ Z_2^{1/2} \ (A_1 + A_2)^{3/2}}{(Z_1^{2/3} + Z_2^{2/3})^{3/4} \ A_1^{3/2} \ A_2^{1/2}}$$

and ξ_e is a constant between 1 and 2 which varies approximately as $Z_1^{1/6}$. (Ormrod et al. 1965).

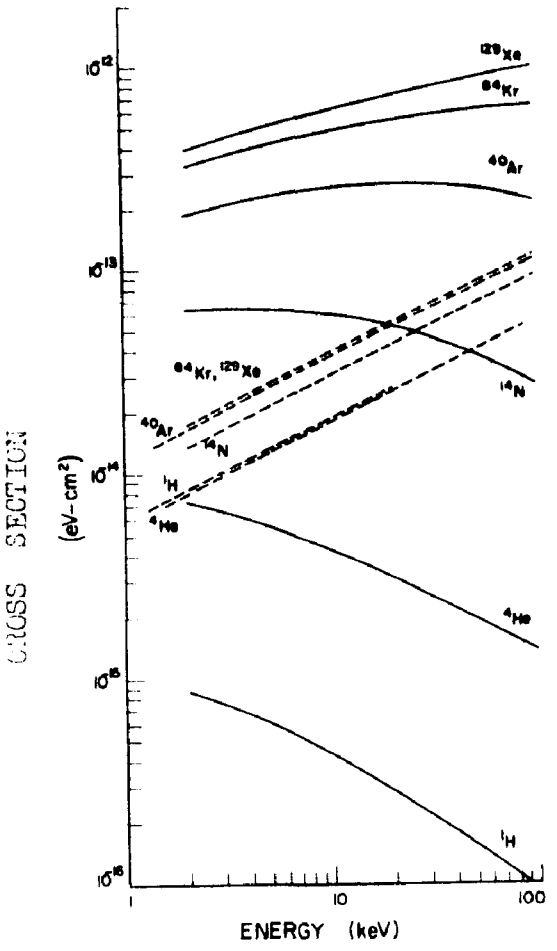

Fig. 2. A logarithmic plot of S_n (solid curves) and S_e (dashed curves) versus energy, for ^{1}H, ^{4}He, ^{14}N, ^{40}A, ^{84}Kr and ^{129}Xe traversing ZnO.

Fig. 2. is a logarithmic plot of S_e and S_n, both as a function of energy for various projectiles in ZnO. The cross sections were first calculated for Zn and O separately and then added. The solid and dashed curves are the nuclear and electronic stopping cross sections, respectively.

It will be noted from the figure that at energies above about 10 KeV $S_e \gg S_n$ for the lighter projectiles whereas for the heavier projectiles the reverse is true. Thus light projectiles lose most of their energy in electronic collisions and heavy ones in nuclear collisions.

ii Experimental Energy Loss Measurements - Recent experiments that fall within the domain of validity of the theory, may be divided into two groups. The first group includes studies of the energy loss of projectiles as they pass through thin films or low pressure gases. The other group includes studies of the ranges of projectiles in various target materials.

In the first group mono-energetic projectiles impinge upon a thin film. The beam emerging from the film is no longer mono-energetic. The total straggling in the energy loss arises from straggling in both the electronic and nuclear energy losses. When, in traversal, energy is lost to electrons only, the projectiles suffer relatively small deflections and both the width of the angular distribution and that of the energy distribution of the projectiles in the emerging beam are small. When the nuclear energy loss becomes important large angle scattering events occur, resulting in a large straggling in the energy loss and a wide angular distribution in the emerging beam. The difficulties involved in precisely measuring the average energy of the emerging beam, taking into account all of the scattered projectiles, are obvious. For the purpose of determining the electronic energy loss, however, only the ions emerging from the film in the direction of the incident beam are energy analyzed and the energy loss in the film calculated (van Wijngaarden and Duckworth 1962, Ormrod et al. 1965 and MacDonald et al. 1966). The projectiles which suffer large angular deflections in nuclear collisions are excluded from observation by collimating slits. Most of the experiments have been limited to projectiles and stopping media for which the nuclear stopping need only be considered as a small correction. Fastrup et al. (1966)

have summarized some of the more recent energy loss measurements for various projectiles, in the mass range 1 - 40 a. m. u., passing through carbon films. In general these measurements agree with theory within the limits of the uncertainty in the constant ξ_e (see Eq. I. A.12). The experimental stopping cross sections exhibit a periodic variation with Z_1, which may depend upon the exact atomic configuration of the projectile and stopping medium, and thus is not predicted by the theory.

No doubt the difficulties involved in determining the total average energy loss, taking into account all scattering events, have limited such measurements in thin targets. To the authors' knowledge the only measurements of this nature were made by Sidenius (1963), who studied the energy loss of heavy ions passing through hydrogen gas. Such an experiment is possible because massive projectiles, in traversing a light stopping medium such as hydrogen, are not deflected appreciably from their original path. The observed results, plotted in terms of ϵ and ρ (see Eq. I. A. 4) showed deviations of about 30 percent from the universal energy loss curve (see Fig. 2). Most of the information concerning the nuclear energy loss has been obtained by the more complicated determination of the range and range straggling of various projectiles in solids.

Many of the range determinations have been summarized by Lindhard et al. (1963b). For amorphous stopping materials good agreement is found between experiment and theory. In the range measurements of Davies and his co-workers (See for example, McCargo et al. 1963, Domeij et al. 1964 and Brown et al. 1965) metal surfaces are bombarded with beams of radio-active ions having energies from 1 KeV to 2 MeV. After the irradiation, successive layers of the bombarded surface are removed and

the residual activity in the sample determined. In this manner the distribution in the penetration depth for various projectiles and stopping media were obtained. For amorphous stopping materials, such as Al_2O_3, these determinations agree well with theory. In crystalline materials the range distributions exhibited a pronounced tail. For such materials the average range could be as much as a factor of four (Davies et al. 1965) greater than the predicted range. This is due to the penetration of the projectiles through open channels in the crystalline lattice of the target. Computer studies of the range in crystalline matter also indicate that the average range may be much greater than the range in amorphous materials (Beeler and Besco 1962) and range measurements in crystalline materials cannot be directly compared to the above theory (Lutz et al. 1965).

B. Luminescence Under Ion Bombardment

When a fast atomic projectile impinges upon a phosphor, light is produced. The variation of the light output with incident ion energy, for various projectiles and different phosphors, has been studied by several authors and in particular by Eve and Duckworth (1958) and van Wijngaarden et al. (1965). Van Wijngaarden et al. (1965) suggested that the light output should be proportional to the total energy loss of a projectile in electronic collisions;

(I. B. 1) $$L(E_o) = K \int_o^{E_o} (S_e / S) dE,$$

where E_o is the incident energy and K should be approximately constant over a relatively small velocity interval. The integral represents the part of the energy lost by a projectile in electronic collisions as it loses its total energy E_o in the phosphor. Good agreement was found

between experiment and Eq. (I. B. 1) for a MgO phosphor.

The origin of the equation may be qualitatively understood as follows. When a phosphor is irradiated with electrons or ultra - violet light, photons are produced as electrons, excited by the radiation, return to the ground state. For small excitations the intensity of the light produced is proportional to the number of excited electrons. It is thus reasonable to assume that the luminescent intensity during ion bombardment is proportional to the energy loss to electrons.

C. Deterioration Under Ion Bombardment

i. The Deterioration Constant - Radiation damage in a phosphor may be observed as a decrease in its luminescent efficiency. Broser and Warminski (1951) studied the relationship between the efficiency of damaged CdS and the number, n, of α particles by which a unit area of the phosphor surface had been irradiated. They found that irradiation caused crystal defects which introduced localized energy levels between the valence and conduction bands of the crystal. The decrease in efficiency was attributed to the presence of these energy levels. Hanle and Rau (1952) adapted Broser and Warminski's treatment to phosphors in which the number of activators is small. They obtained the relation.

(I. C. 1)
$$\frac{L}{L_o} = \frac{1}{1 + C'n} ,$$

where L is the light output after irradiation by n particles per unit area and L_o is the light output prior to bombardment. C' is the deterioration constant, which depends upon the type of phosphor and the projectile. Hanle and Rau found the relation to hold accurately for ZnS:Ag

and approximately for Zn_2SiO_4:Mn and $MgWO_4$. Table I lists the observed C' values for various projectiles with energies of about 25 KeV. The deterioration constants were reported to be independent of energy, in disagreement with the present work, in the range of energy from 15.2 to 29.7 KeV.

TABLE I

The Deterioration Constants, C',
at about 25 KeV. (from Hanle and Rau, 1952)

Phosphor	H_2^+	He^+	Ne^+	Ar^+	Xe^+
ZnS:Ag	$.045 \times 10^{-11}$	$.23 \times 10^{-11}$	$.92 \times 10^{-11}$	$.95 \times 10^{-11}$	$.98 \times 10^{-11}$
Zn_2SiO_4:Mn	$.002 \times 10^{-11}$	$.012 \times 10^{-11}$	$.08 \times 10^{-11}$	$.14 \times 10^{-11}$	$.19 \times 10^{-11}$
$MgWO_4$	$.002 \times 10^{-11}$	$.005 \times 10^{-11}$	$.14 \times 10^{-11}$	$.19 \times .0^{-11}$	$.27 \times 10^{-11}$

Eq. (I. C. 1) may be derived with the aid of Figs. 3(a) and 3(b), which indicate the energy band scheme of a phosphor before and after irradiation, respectively. In these figures C and G represent the conduction and valence bands and A and D represent the position of localized energy levels associated with the activators and crystal defects respectively. These symbols have a numerical value equal to the number of their respective energy levels per unit volume. n^- is the number of electrons in C and a^+ and n^+ are the number of holes in A and G respectively. If a hole-electron pair is created by the excitation of an electron from G to C, the direct transition of the electron back to G is forbidden. The hole will migrate through the lattice until it is trapped by an activator. The electron in C may now make a transition to G, via A, emitting a photon

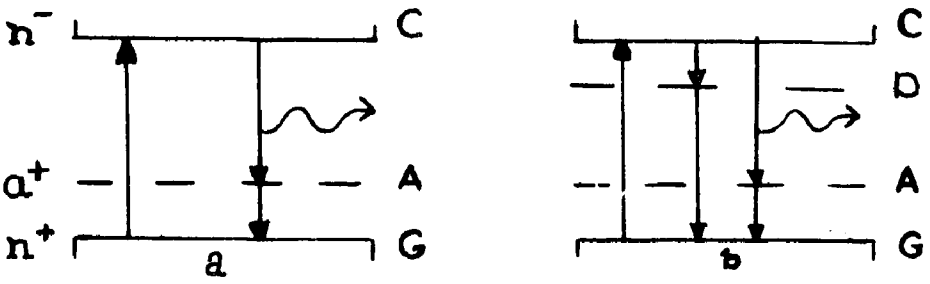

Fig. 3. a) Band model for undeteriorated ZnO phosphor. n^- is the electron population of the conduction band C and a^+ and n^+ are the hole populations of the activator centres, A and the valence band G, respectively. The arrows show allowed transitions.

b) Band model for a damaged ZnO phosphor. The energy levels, D, are associated with crystal defects.

in the process. In the damaged phosphor the excited electron can return to the ground state either via an activator level, thus producing a photon, or via a defect level D, by means of a (so called) radiationless transition.

When an undamaged phosphor is subjected to constant irradiation, which excites Z_o electrons, in unit volume, per second into the conduction band, then at equilibrium there will be a total emission of Z_o photons per second.

The rate of photon emission is given by,

(I. C. 2) $$Z = \beta\, n^-\, a^+,$$

where β is the probability for a transition from C to G via A. In the damaged phosphor the radiationless transitions compete with those producing visible light. In this case the rate of change of the number of electrons in the conduction band is given by

(I. C. 3) $$dn^- / dt = Z_o - \beta\, n^-\, a^+ - \delta\, Dn^-,$$

where δ is the probability for a transition from C to G via D. At Equilibrium the preceeding equation yields

(I. C. 4) $$\beta\, n^-\, a^+ = Z_o - \delta\, Dn^-.$$

Substitution of Eq. (I. C. 2) into Eq. (I. C. 4) yields,

(I. C. 5) $$Z / Z_o = 1 / (1 + \delta D / \beta a^+) .$$

If the number of activators is small, all of them are activated and $a^+ = A$. The value Z / Z_o equals the relative efficiency, η / η_o, of damaged to undamaged phosphor, and Eq. (I. C. 5) may be written as,

(I. C. 6) $$\eta / \eta_o = 1 / (1 + \delta D / \beta A) .$$

This equation is valid for a phosphor in which D and A are uniform. When a thin layer of phosphor is deteriorated by energetic projectiles, the energy of the projectiles, during traversal, is essentially constant. In this layer the number of defects produced per unit volume is $D = nd$, where d is the number of defects produced in unit path length per projectile and n, the irradiation dose, is the number of projectiles that have impinged upon a unit area of the phosphor surface. Thus Eq. (I. C. 6) becomes,

(I. C. 7) $$\eta / \eta_o = 1 / (1 + Cn) ,$$

where

(I. C. 8) $$C = \delta d / \beta A.$$

The physical significance of the deterioration constant is that it represents a cross section, with dimensions of area, whose value is directly proportional to the number of defects produced per unit distance along the projectile trajectory..

It is interesting to compare the deterioration constant, C, derived above, to Hanle and Rau's C' values. To do this it must be assumed that the number of defects introduced by a heavy atomic projectile are uniformly distributed over its range. If an average energy of about

25 eV is needed to produce a defect, then a 25 KeV projectile, which loses most of its energy in nuclear collisions, introduces about 10^3 defects. In doing so, it travels a distance of the order of 5×10^3 A^o. Thus $d \simeq 10^7$ cm^{-1}. For ZnS:Ag Hanle and Rau quote an impurity concentration $A = 2.52 \times 10^{18}$ cm^{-3}. From the work of Broser and Warminski (1951) it is found that β and δ have the same order of magnitude in ZnS. When the order of magnitude estimates are substituted into Eq. (I. C. 8) it is found that $C' \simeq 10^{-11}$, the same order of magnitude (see Table I) as the C' values for the heavier ions. As expected the observed values of C' decrease with decreasing projectile mass, since in the KeV energy range light projectiles (^1H and ^4He) lose most of their energy to electrons and thus are much less efficient in producing defects (Young 1955) than the more massive projectiles.

Hanle and Rau's C' values were determined by measuring the ratio, L / L_o, for projectiles impinging upon a phosphor sample with incident energies of about 25 KeV. The damage at the surface of the sample was produced by projectiles at their incident energy, whereas the damage near the end of their range was produced by projectiles with energy near zero. Thus, if the deterioration constant is energy dependent, the resultant damage will not be uniformly distributed over the range of the projectile. The amount of light produced by a projectile is also energy dependent, being larger for higher projectile energies. Therefore, during deterioration, an appreciable fraction of the light is produced near the surface and the ratio L / L_o is determined to a large extent by the properties of the deteriorated phosphor near the surface.

In the present work we found that [see (VIB)] the surface of

ZnS:Ag is much more deteriorated after irradiation than the bulk of the damaged phosphor beneath it. Thus for this phosphor the observed C' values do not correspond to the average damage.

ii The Displacement Cross Section. When a projectile traverses a stopping medium it transfers energy, through nuclear collisions to the stopping atoms and if the energy transfer to such an atom is greater than some minimum value, E_d, the struck atom will be displaced from its lattice position. The value of E_d, the so called displacement energy, varies for different media and is of the order of 25 eV for many materials. An atom directly displaced by the projectile is called a primary. If the displaced atom has sufficient energy it may cause secondary displacements which in their turn may cause tertiary displacements, etc.

For a monatomic stopping medium, Holmes (1962) has studied the number of displacements, $\nu(T)$, which occur when an incident projectile transfers energy T to a primary. $\nu(T)$ is given by,

$$\text{(I. C. 9)} \qquad \nu(T) = \begin{cases} 0 & T < E_d \\ 1 & E_d \leq T \leq 2E_d \\ T/2E_d & T \geq 2E_d \end{cases}$$

For $T \geq 2E_d$ the expression for $\nu(T)$ has been obtained by assuming the collisions between a primary and a secondary, etc. to be of the hard sphere type. More accurate discriptions for $\nu(T)$ (Robinson 1965; Felder and Kostin 1966; Kostin 1966) take the actual scattering in these collisions into account. The expression however, should be approximately valid when E_d is taken to be an empirical constant (Lindhard et al. 1963a). For this reason and because of its simple form, Relation (I. C. 9) for $\nu(T)$ will be used in this dissertation.

If the differential cross section, for the transfer of energy T by a projectile with energy E, is $d\sigma(T, E)$, then the cross section for producing one displaced atom is,

(I. C. 10) $$\sigma_d(E) = \int_0^{T_m} \nu(T)\, d\sigma(E, T),$$

where

(I. C. 11) $$T_m = 4 M_1 M_2 E / (M_1 + M_2)^2,$$

is the maximum energy transfer in a head on collision. Substitution of Eq. (I. C. 9) into Eq. (I. C. 10) yields,

(I. C. 12) $$\sigma_d(E) = \int_{E_d}^{2E_d} d\sigma(E, T) + \int_{2E_d}^{T_m} T/2E_d\, d\sigma(E,T).$$

In Appendix I. the nuclear stopping cross section,

(I. C. 13) $$S_n = \int_0^{T_m} T\, d\sigma(E,T)$$

and σ_d are compared for a monatomic stopping medium, whose mass and atomic number are $M_2 = 42$ and $Z_2 = 19$, the average values of these quantities for Zn and O. The values of S_n and σd were found by numerical integrations using a graphical representation for $d\sigma$ given by Lindhard et al (1963). It is shown that for heavy projectiles

(I. C. 14) $$\sigma_d \cong S_n / 2 E_d$$

For lighter projectiles σ_d is somewhat smaller than $S_n / 2 E_d$, the maximum discrepancy occuring for ^1H where $\sigma_d \cong .8\, S_n / 2 E_d$. It will be assumed that the form of Eq. (I. C.14) holds for a ZnO stopping medium even though, strictly speaking, Eq. (I. C. 9) is valid only for a stopping medium consisting of a single atomic species.

The total number of displacements, introduced by a projectile per unit distance along its path in a medium of atomic density N is $d = N \sigma_d$. Substitution of this relation into Eq. (I.C.3) yields,

$$C = \frac{\delta \sigma_d N}{\beta A} . \qquad \text{(I. C. 15)}$$

An approximate relation [see Eq. (I. C. 14)] is

$$C \simeq \frac{\delta N S_n(E)}{2 \beta A E_d} \qquad \text{(I. C. 16)}$$

which should be quite accurate for heavier projectiles.

CHAPTER II

APPARATUS

Fig. 4 is a schematic diagram of the apparatus. Ions produced in an electron bombardment source (see, for example, Duckworth 1958) are accelerated between slits S_1 and S_2 by a high voltage power supply, H. V. (Sorensen model 2150 Rand D), which has a continuously variable output between 1 and 150 KeV, calibrated to an accuracy of $\pm$ 1/2 per cent. After acceleration the beam, collimated by slit S_3, enters a magnetic field, B, for separation into its mass components. The desired mass is bent through an angle of 30° along a circular path of 35 in. radius. The beam is then further collimated by slit S_5 and collected by a Faraday cup, F. Slit S_6 is maintained at a negative potential of 90 V to prevent the escape of secondary electrons from the Faraday cup. The beam current is measured, to a relative accuracy of about $\pm$ 1/2 percent, by means of an electrometer (Keithly, model 417) connected to the cup. The dimensions of slits S_1, S_2 and S_3, are .020 in. by .50 in. and those of S_6 are .10 in. by .50 in. Slit S_5

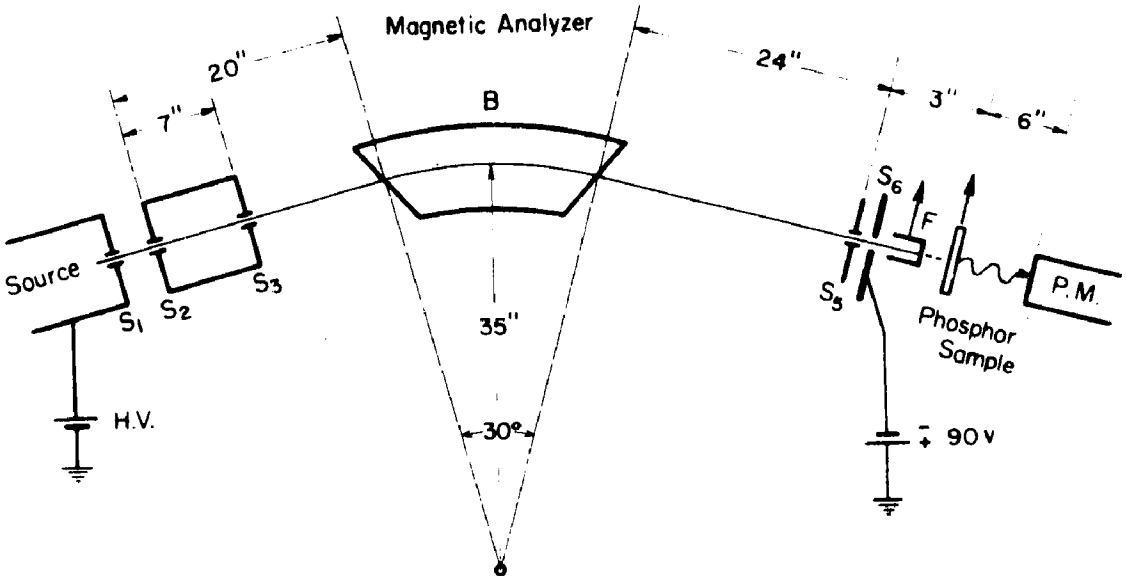

Fig. 4. Schematic diagram of apparatus.

is constructed in such a manner that its dimensions may be alternately .030 in. by .250 in. or .015 in. by .150 in. in order to obtain ion beams of different cross sectional areas. The divergence of the ion beam is sufficiently large to produce an approximately uniform ion distribution over the area of S_6, when it has either set of dimensions. The resolution of the instrument, with the smaller exit slit dimensions was observed to be about one part in one hundred at the base of the mass peaks.

The Faraday cup could be removed from the path of the ion beam by means of a bellows system. This allowed the beam to impinge upon a sample which consisted of tiny phosphor crystals deposited, to a depth of a few tenths of a millimeter, on a microscope slide. To prevent the phosphor from charging up during irradiation, the glass backing had been previously coated with a highly conducting but practically transparent film of CdO. The phosphor sample was mounted by means of a bellows system so that it could be moved in an arc perpendicular to the ion beam. This arrangement permitted the locking of the phosphor sample in up to sixteen fixed positions relative to the beam and also the rapid scanning of the sample across the beam. Light produced during irradiation of the sample was monitored by means of a photomultiplier tube, P.M. (Philips, 153 AVP). The output of the photomultiplier was measured to a relative accuracy of $\pm$ 1/2per cent by means of a Keithly electrometer (model 621). Provision was made for the insertion of optical filters between the phosphor sample and the photomultiplier.

Fig. 5 is a composite plot of the response of the photomultiplier and the emission spectrum of ZnO:Zn (Sylvania type 137). The dashed curve is the sensitivity of the photomultiplier, in arbitrary units, as a function

of the wavelength of incident light. The solid curve, obtained from the Sylvania catalogue, is the intensity of luminescence of ZnO:Zn versus wavelength, also in arbitrary units. It is apparent from the figure that the phosphor exhibits two peaks in its luminescent spectrum, which, however, both fall within the range of sensitivity of the photomultiplier.

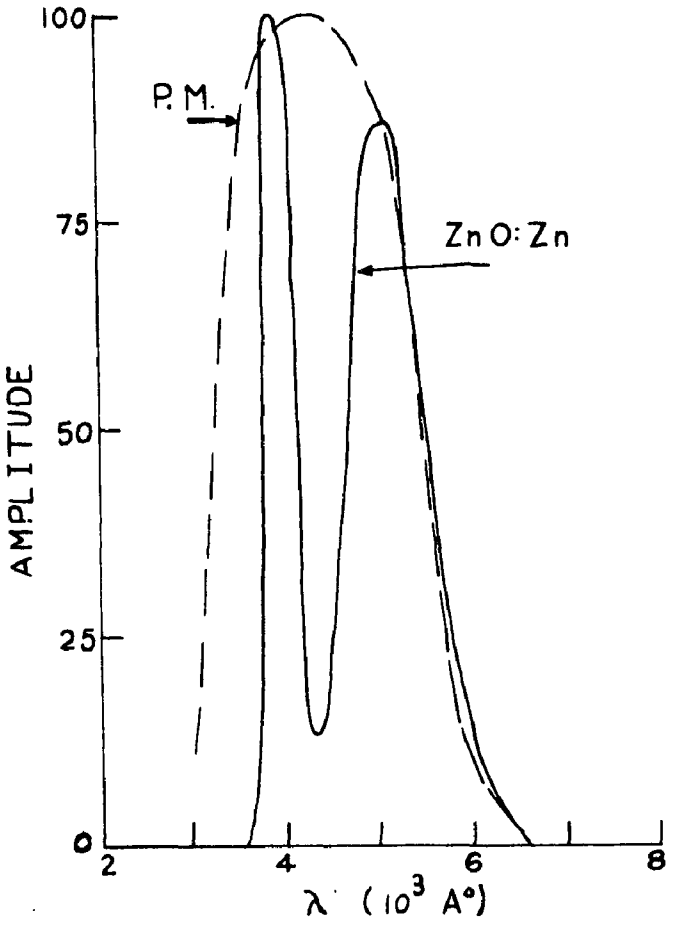

Fig. 5. Composite plot showing the luminescent intensity of ZnO:Zn (solid curve) and the sensitivity of the photomultiplier (dashed curve), both in arbitrary units, versus wavelength.

The phosphor samples were prepared by first suspending the tiny (~ 4 micron) ZnO:Zn crystals in alcohol. This suspension was then poured into a container with the microscope slide near the bottom. The phosphor particles then settled from the mixture, thus forming an even

coating on the surface of the slide. The alcohol was then drained away and the sample allowed to dry.

The rate of deposition of the phosphor from the suspension varies with the particle size, being slower for the smaller particles. Thus the average size of the particles at the surface of a sample was smaller than the average size of the phosphor particles. Although care was taken to prepare different samples under similar conditions, the average particle size in the surface layer is believed to have differed slightly from sample to sample.

CHAPTER III

ENERGY LOSS

A. Technique

The determination of the energy loss in ZnO:Zn for various projectiles is carried out in two steps. Local regions on the surface of a phosphor sample are deteriorated (I. C.) by beams of low energy ($\sim$ 5 KeV) heavy ions, with large currents. The deterioration is performed with the exit slit, S_5, opened to its larger dimensions. In this manner 'thin films' of highly deteriorated phosphor, equal in area to that of the exit slit and with thicknesses of the order of 10^2 A^o, are produced. For a sufficiently large irradiation dose these films do not luminesce under ion excitation.

After the preparation of the thin films the exit slit is reduced to its smaller dimensions and the sample is scanned across an ion beam, whose energy loss in traversing the films is to be determined. The smaller cross sectional area of the scanning beam ensures that all the ions in the beam will impinge upon a thin film, allowing the determination of the energy loss of the beam with greater certainty. To guard against further deterioration of the phosphor, the beam current is kept as small as possible and the sample is scanned rapidly across the beam. Fig. 6 is an illustrative diagram of a phosphor sample, deteriorated in 5 local regions, showing the relative cross sectional areas of the deteriorating and scanning beams.

The energy loss of the projectiles is determined by measuring the light intensities produced by the projectiles impinging upon fresh phosphor and by those which first traverse a deteriorated film.

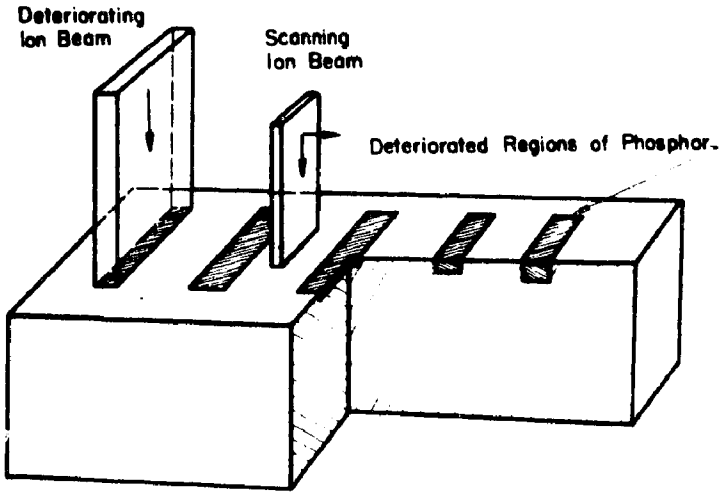

Fig. 6. Schematic diagram of a damaged phosphor sample showing depths of deterioration (not to scale) for various damaging beams. The cross sectional areas of the damaging and scanning beams are indicated.

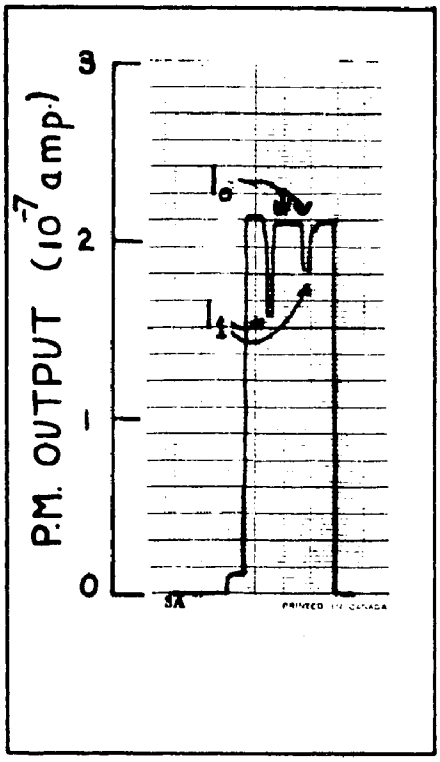

Fig. 7. A reproduction of a recorder tracing showing the photomultiplier output as the sample is scanned across a 35 KeV $^4He^+$ beam with a current of 1.75×10^{-12} amp. The left and right dips marked I_1 correspond to the light produced after the beam has traversed regions deteriorated with 7.8 and 3.2 KeV CO_2^+, respectively. I_o corresponds to the light produced in undeteriorated phosphor.

B. The Energy Loss of Various Projectiles

Two local regions of a ZnO:Zn phosphor sample were deteriorated by 1.2×10^{14} CO_2^+ ions cm^{-2} at energies of 7.8 and 3.2 KeV, respectively. During irradiation the light output of the phosphor decreased to about one percent of its initial value. The relative efficiency, of the damaged to undamaged phosphor, was considerably lower than this since, near the end of the deterioration process, most of the light is produced by ions in the edge of the beam traversing fresh phosphor (Hastings et al 1967).

The sample was then scanned across beams of various projectiles and the photomultiplier output recorded. Fig. 7 is a reproduction of a typical recorder tracing of the integrated photomultiplier output current versus the distance along the phosphor surface for a ^4He beam with an incident energy of 35 KeV. The vertical scale indicates the observed photomultiplier output current. The flat region of the tracing corresponds to ℓ_o, the photomultiplier current observed when the beam impinged upon undeteriorated phosphor. The left and right 'dips' correspond to the current ℓ_1, observed for the beam traversing the regions deteriorated by the 7.8 and 3.2 KeV CO_2 ions, respectively. Division of ℓ_o and ℓ_1 by the incident ion current yields L_o and L_1, measures of the light output per incident ion, and hereafter referred to as the light outputs.

Fig. 8 is a plot of L_o and the L_1's for the two films versus E_o, the incident ^4He energy. For a given light output, the difference in energy, ΔE, between L_o and either of the L_1's, is the total average energy loss of ^4He in traversing the corresponding film, at an

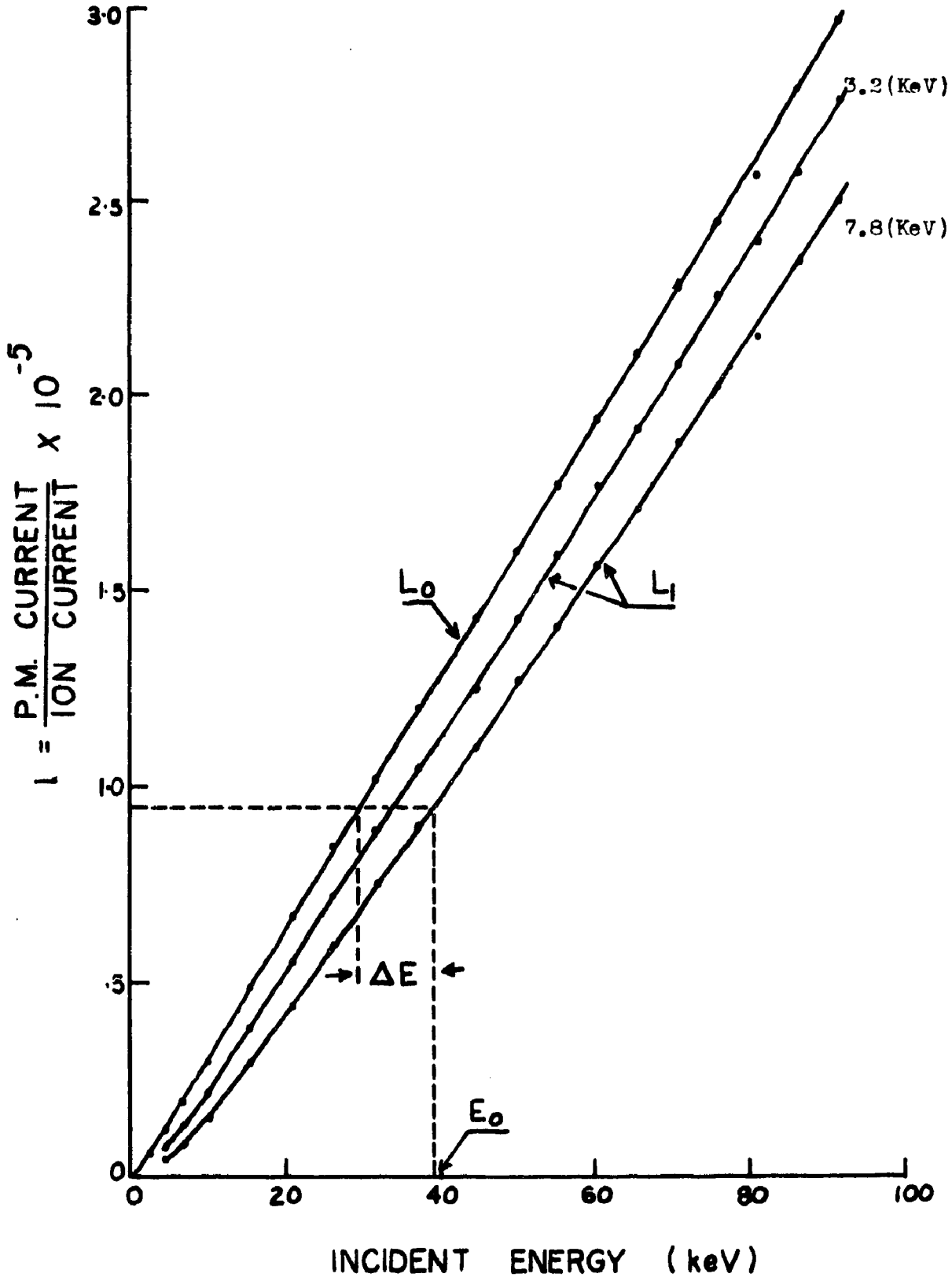

Fig. 8. A composite diagram showing the light output L_0 of undeteriorated ZnO:Zn_+ and the L_1's for regions damaged with 7.8 and 3.2 KeV CO_2, all as a function of the incident $^4He^+$ energy.

average energy $E = E_o - \Delta E / 2$. The curves marked ^4He in Fig. 9 are logarithmic plots of ΔE versus E as read from Fig. 8. The circles and crosses correspond to the energy loss in the 7.8 and 3.2 KeV CO_2 films, respectively. The curves marked ^{40}Ar and ^{84}Kr present the observed energy losses for these projectiles in the same films. Fig. 10, which is similar to Fig. 9, presents the observed ΔE values for ^1H and ^{14}N. Since the uncertainties in the energy losses of hydrogen in the thinner film were very large, these measurements have not been included in the figure.

The error in the energy loss curves depended upon the accuracy to which the experimental points, in plots similar to Fig. 8, for L_o and L_1, could be determined. The relative errors in the photomultiplier current, the ion current and the high voltage are about $\pm$ 1/2 percent each, thus the total error in the experimental points is less than $\pm$ 2 percent. The error in the line of best fit drawn through the points is thus expected to be less than $\pm$ 1/2 percent. The error in the energy loss, however, depends on its magnitude. At 60 KeV the error in ΔE is at most about $\pm$ .6 KeV. Thus the maximum errors in the energy losses for ^1H, ^4He, ^{14}N, ^{40}Ar and ^{84}Kr are estimated to be $\pm$ 17 percent, $\pm$ 12 percent, $\pm$ 5 percent, $\pm$ 3 percent, and $\pm$ 2.5 percent, respectively, in the thinner film. In the thicker film the error is approximately half of this.

It will be noted that the energy loss curves for any particular projectile (Fig. 9 and Fig. 10), for the two films, are parallel within the limits of experimental error, indicating that the energy loss in the thicker film is a constant multiple, independent of energy, of that in the thinner film. The second column in Table 2 lists the ratios of the energy losses in the two films for the projectiles listed in the first

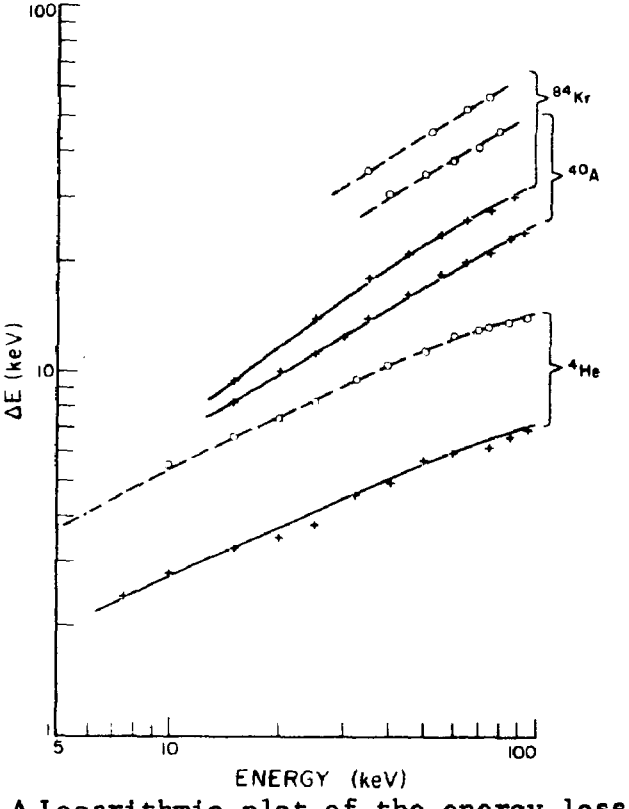

Fig. 9. A Logarithmic plot of the energy loss, ΔE, versus the energy for ^{4}He, ^{40}A and ^{84}Kr traversing films of $^{+}$ZnO:Zn deteriorated with 7.8 KeV CO_2^{+} (circles) and 3.2 KeV CO_2^{+} (crosses).

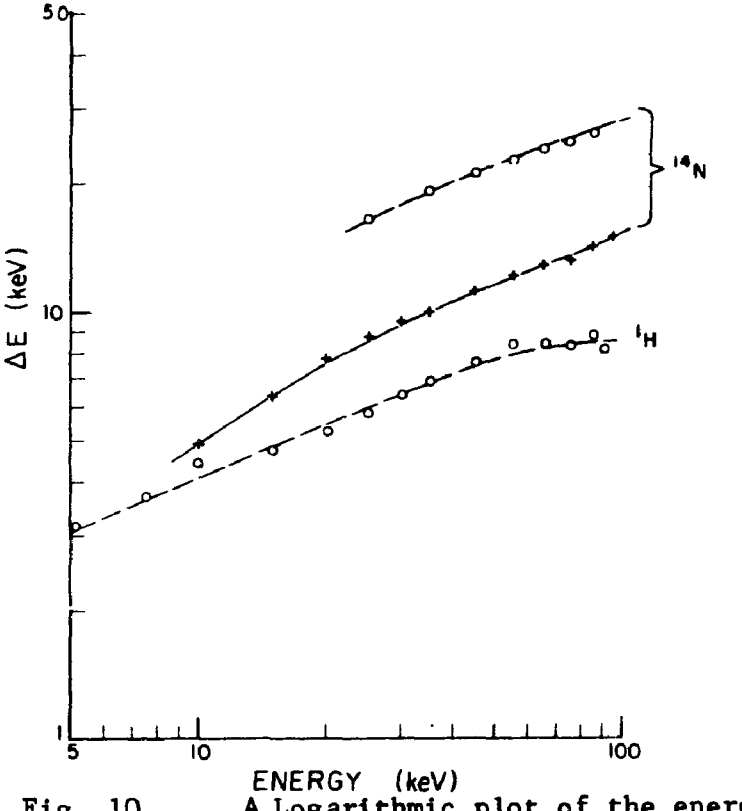

Fig. 10. A Logarithmic plot of the energy loss of ^{1}H and ^{14}N. The circles and crosses are the observed energy losses in the 7.8 and 3.2 KeV CO_2^{+} film respectively.

column. These ratios are the same, within experimental error, having an average value of 1.99.

TABLE II

The Ratio of the Energy Loss in the Thicker Film to that in the Thinner Film for Various Projectiles

Projectile	Ratio of Energy Losses
^{4}He	2.04
^{14}N	1.87
^{40}Ar	2.02
^{84}Kr	2.01

The fact that the energy loss in the thicker film is a constant multiple of that in the thinner film implies that our films are thin and that $\Delta E / t$, the ratio of the energy loss to the film thickness, is independent of t. By extrapolation it follows that $\Delta E / t$ should remain constant as $t \to 0$. Thus for our films (of finite thickness) $\Delta E / t$ equals $\lim_{t \to 0} \Delta E / t$, the stopping power. Thus

(III. B. I) $$-dE / dR \simeq \Delta E / t \quad .$$

C. Estimate of Film Thickness

In the present experiments no attempt was made to measure the film thicknesses (i. e. the depth of the deteriorated regions). An estimate, however, was made using the energy loss of hydrogen.

In the KeV range ^{1}H loses most of its energy to electrons

[see (I. A.)]and below about 25 KeV the observed electronic stopping cross sections generally agree quite well with theory. Thus it was assumed that the theoretical stopping cross section for hydrogen in ZnO is also reasonably valid. Substitution of Eq. (III. B. 1) into Eq. (I. A. 3) yields,

(III. C. 1) $$t \simeq \Delta E / NS \qquad E < 25 \text{ KeV},$$

where ΔE and S are the observed energy loss and theoretical stopping cross section for ^1H. Substitution of the observed energy loss from Fig. 10 and S from Fig. 2, both at 10 KeV, and the molecular density of ZnO, $N = 4.15 \times 10^{22}$, yields $t \simeq 525$ A° for the thickness of the thicker film. Division of this by 1.99 the ratio of the film thicknesses yield $t \simeq 265$ A° for the thinner film.

D. Comparison to Theory

The energy losses for the various projectiles in the thinner film have been summarized in Fig. 11. The crosses represent the energy losses observed in the 3.2 KeV CO_2 film and the circles represent the observed energy losses for hydrogen in the 7.8 KeV film, divided by 1.99, the ratio of the film thicknesses. The solid curves represent the predicted energy losses in a 265 A° ZnO film, obtained by means of Eq. (I. A. 3) and Fig. 2. It will be noted that, relative to hydrogen, the discrepancy between the observed and theoretical total energy losses, increases with projectile mass and decreases with increasing projectile velocity. Since the heavy projectiles lose most of their energy through nuclear collisions it appears that the Lindhard theory overestimates the nuclear energy loss, when applied to crystalline materials, at low velocities.

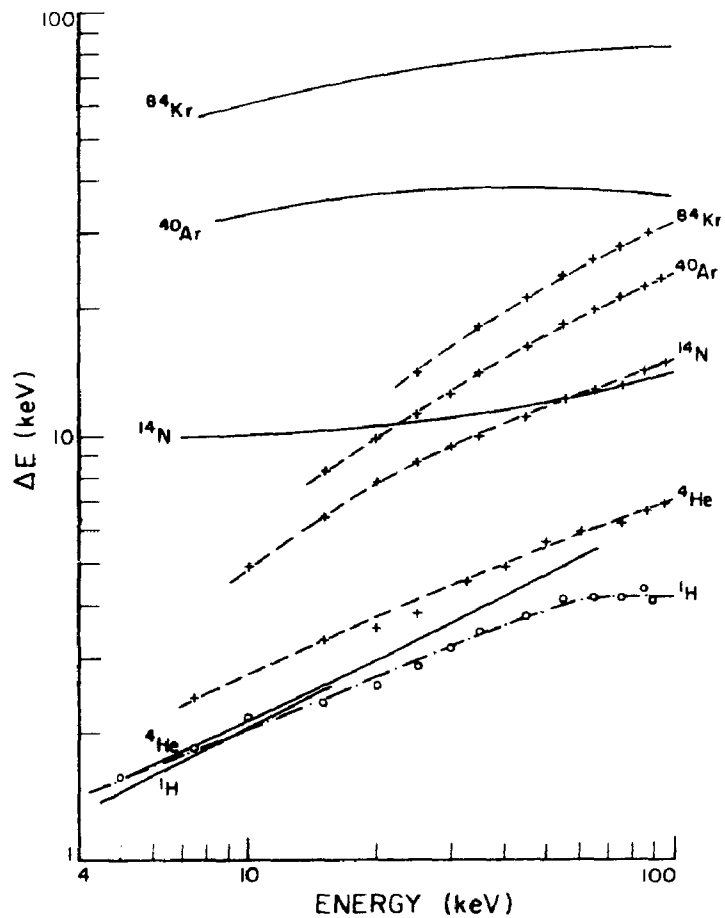

Fig. 11. A logarithmic plot of the energy loss versus energy for ^{1}H, ^{4}He, ^{14}N, ^{40}A and ^{84}Kr in traversing a 265A° film of ZnO:Zn. The dashed curves are drawn through the experimental points and the solid curves are theoretical (see text).

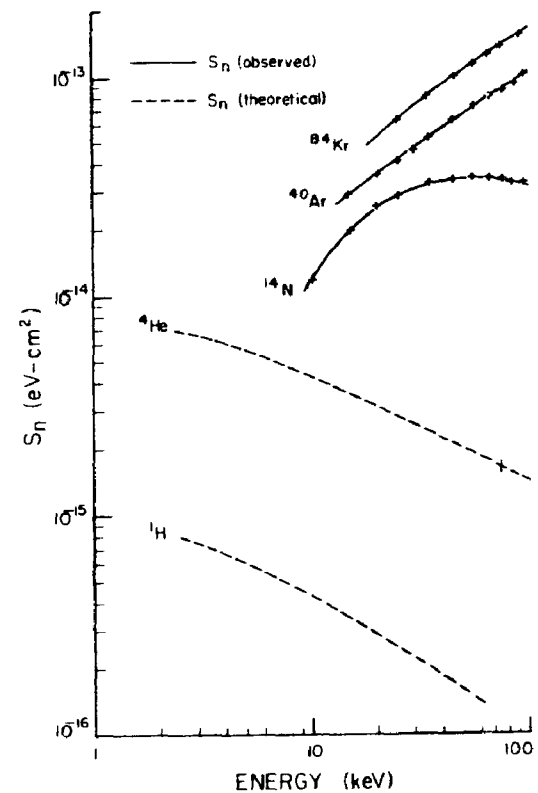

Fig. 12. A logarithmic plot of S_n versus energy for ^{1}H, ^{4}He, ^{14}N, ^{40}A and ^{84}Kr in ZnO:Zn. The solid curves are experimental and the dashed ones theoretical (see text).

The effective total stopping cross sections may be obtained by dividing the observed average energy losses by the molecular density and the estimated film thickness. The effective nuclear stopping cross sections, for the heavier projectiles may then be obtained using the relation,

(I. A. 2) $$S_n = S - S_e$$

where S is the observed total stopping cross section and S_e is the theoretical electronic stopping cross section. S_n obtained in this manner should be fairly accurate since the predicted electronic stopping cross section has been found to be quite reliable in several stopping media (Fastrup et al. 1966, MacDonald et al. 1966). Moreover the magnitude of the nuclear stopping cross section for the heavier ions is appreciably larger than that of the electronic stopping cross section, thus small uncertainties in the latter do not introduce large errors in the former. Fig. 12 is a logarithmic plot of the 'observed' S_n values versus energy for ^{14}N, ^{40}Ar, and ^{84}Kr. The figure also includes the theoretical S_n curves for ^{1}H and ^{4}He.

E. Discussion

It has been found that the observed nuclear energy loss is considerably lower (as much as a factor of 4) than the theoretical one for low projectile velocities. This may be due to the fact that the stopping medium is not truly amorphous but consists of tiny ZnO:Zn crystals in which the average nuclear energy loss may be reduced by channeling or some related effect.

The question may arise as to whether the presence of the damaging projectiles in the thin films has altered their effective stopping

cross sections. Since the total irradiation dose is less than the number of atoms per unit area in a mono-layer of the stopping material, it is concluded that the presence of these atoms did not significantly affect the observed stopping cross section.

CHAPTER IV

IONOLUMINESCENCE OF ZnO:Zn

On excitation ZnO:Zn exhibits two peaks in its luminescent spectrum (see Fig. 4) and the question may arise as to whether this spectrum shifts with a change in ion energy or ion mass. The following experiments were designed to test this and also the validity of Eq. (I. B.1);

$$L_o(E_o) = K \int_o^{E_o} S_e / S \, dE \,. \qquad \text{(I. B. 1)}$$

A phosphor sample was scanned across beams of ^{1}H, ^{4}He, ^{14}N, ^{20}Ne, ^{40}Ar, ^{84}Kr and ^{129}Xe, in this order, and the light output per unit ion current, L_o, was observed with and without an optical filter interposed between the sample and the photomultiplier. The filter had a transmission band centred at about 5500 A^o. Fig. 13 is a logarithmic plot of L_o versus the incident energy, E_o, of the scanning beam, for the various projectiles. The circles correspond to the experimental points obtained without a filter, whereas the crosses correspond to 14.5 times the light values obtained with the filter in position. This normalization factor made the curves drawn through the crosses and squares coincide.

To ensure that the phosphor did not deteriorate to any noticeable degree during the irradiation, the sample was scanned across the beam as rapidly as possible and the ion current kept to the necessary minimum. To check that the phosphor sample had not been significantly deteriorated during these experiments, a new sample was scanned with ^{1}H and ^{129}Xe and the relative magnitudes of the L_o curves, so obtained, were compared to those in Fig. 13. There was no discrepancy, within experimental error, between the two sets of data, showing that the light outputs,

for the various projectiles, are representative of undeteriorated ZnO:Zn.

The energy dependence and the relative magnitudes of the light outputs without the filter are the same as those obtained with the filter in position. This was taken to indicate, in agreement with observations for other phosphors (van Wijngaarden et al. 1965), that the distribution in the spectral response of the phosphor is independent of ion energy and ion mass.

The curves in the log-log plot of Fig. 13 are approximately linear showing that the light outputs vary as the energy raised to a

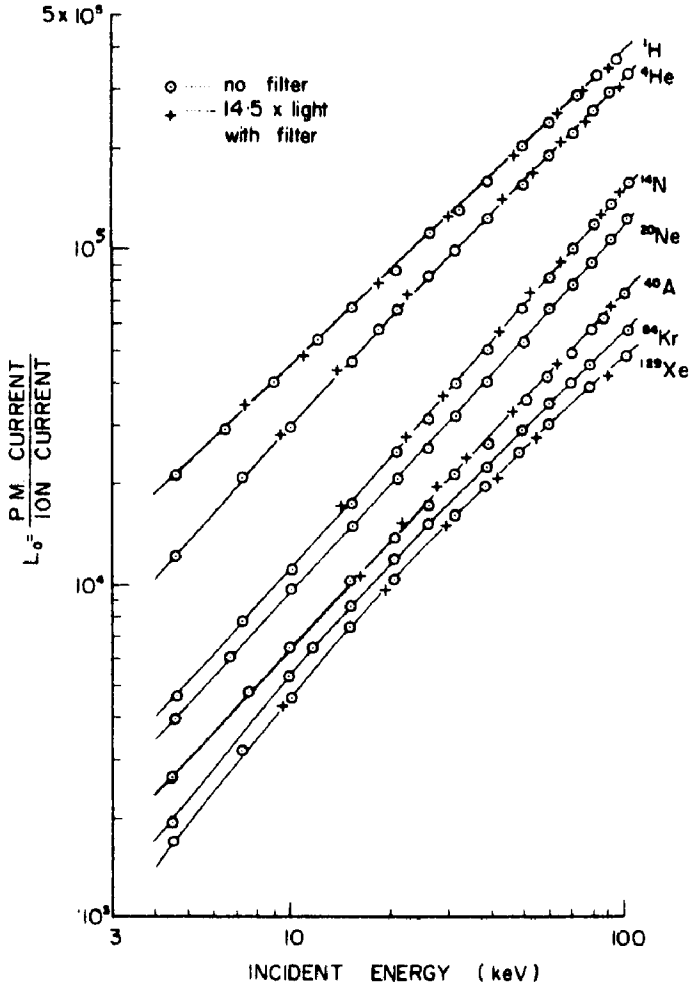

Fig. 13. The light output versus energy for various projectiles impinging upon ZnO:Zn. The crosses are 14.5 times the light outputs observed with a filter interposed between the sample and photomultiplier. The circles correspond to the light observed without the filter.

power, equal to the slope of the curves. Table III lists these exponents, at about 60 KeV, which do not deviate significantly from unity. Thus the light output is approximately proportional to the incident energy.

TABLE III

The Exponents for the Light Output, At About 60 KeV as Expressed in the Equation $L_o \propto E_o^P$

Projectile	^1H	^4He	^{14}N	^{40}Ar	^{84}Kr
Exponent	.97	1.04	1.17	1.10	.95

To compare the observations to Eq. (I. B. 1), the ratios S_e / S have been plotted versus energy in Fig. 14, for the various projectiles. S is the observed total effective stopping cross section, obtained from Fig. 11 using Eqs. (I. A. 3) and (III. B. 1) and S_e is the

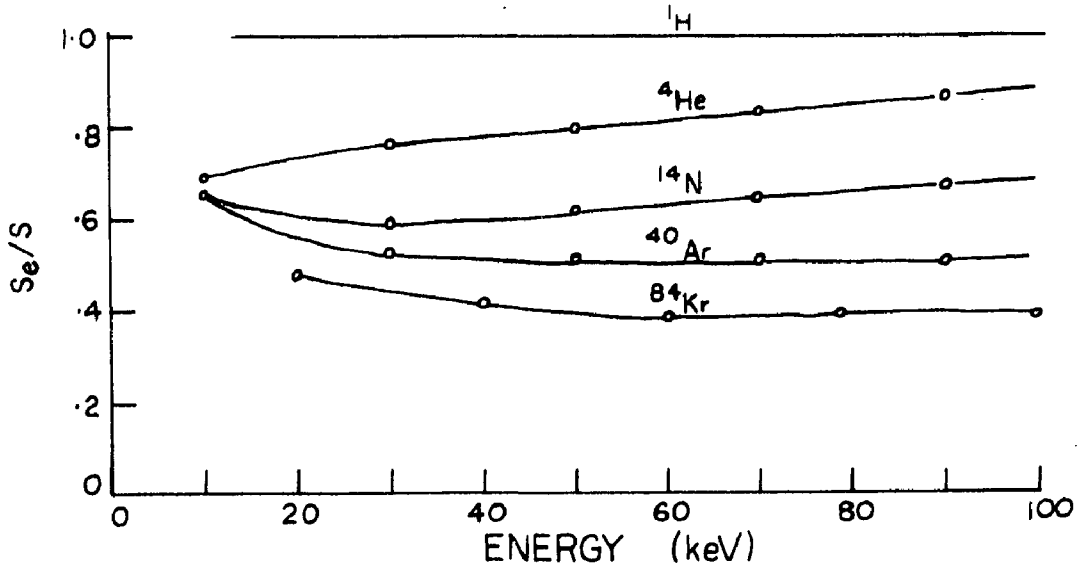

Fig. 14. A plot of S_e / S versus E for various projectiles. For ^1H it was assumed that $S_e = S$ while for the other projectiles S_e and S are the theoretical electronic and the observed total stopping cross sections respectively.

theoretical electronic stopping cross section for all the projectiles except hydrogen. For hydrogen S_e was taken to be equal to the observed total stopping cross section. It will be noted that S_e / S is almost a constant, independent of energy, in the range of energies studied, for all projectiles. Thus to a first approximation, Eq. (I. B. 1) indeed predicts the correct energy dependence of L_o.

Since S_e / S does not vary rapidly with energy the difference in the light outputs for two incident energies [see Eq. (I. B. 1)] is approximately given by

$$\Delta L = K\,(S_e / S)\,(E_1 - E_2). \qquad \text{(IV. 1)}$$

The ΔL values predicted by this equation are compared to the observed ΔL values in Table IV. The second column lists the observed ΔL values for the energy interval 20 to 100 KeV, relative to hydrogen, for several projectiles listed in the first column. The last column presents the theoretical ΔL values also relative to hydrogen for a common K value. The differences between the predicted and observed ΔL values show that Eq. (I. B. 1) does not predict the relative magnitudes of the light outputs even though it predicts the correct energy dependence.

TABLE IV

Observed and Theoretical ΔL Values in the Energy Interval 20 to 100 KeV.

Projectile	$\Delta L_{obs.}$	$\Delta L_{theor.}$
^{1}H	1	1
^{4}He	.82	.81
^{14}N	.42	.63
^{40}Ar	.19	.51
^{84}Kr	.15	.43

The discrepancy may indicate that K is a velocity dependent function that should have been included under the integral sign. The reason for this may be understood by considering the maximum energy that a heavy projectile can transfer to an electron. When a heavy ion collides with an electron the maximum velocity that can be imparted to the electron is twice the velocity of the ion. Thus the fraction of the total number of excited electrons, which reaches the conduction band, decreases with decreasing projectile velocity and at lower velocities the relative efficiency of light production decreases.

CHAPTER V

THE DETERIORATION DEPTH

A. Technique

The depth to which a phosphor is deteriorated after prolonged irradiation by a large number of particles depends upon the incident energy of the damaging beam and, to some extent, upon the irradiation dose, n. To systematically investigate the deterioration depth several local regions on ZnO:Zn phosphor samples were deteriorated at different energies and with various irradiation doses until the light output was reduced to less than 1% of its initial value. After the irradiation the deterioration depth, D, was determined by ameasurement of the energy loss at 60 KeV of a ^{1}H beam in traversing the damaged regions. D is related [See Eq.(III.B.1)] to ΔE approximately as

(V.A.1) $$D = (-dE/dR)^{-1} \Delta E$$

where $-dE/dR$ is the stopping power for ^{1}H at 60 KeV. At this energy $-dE/dR$ varies only slowly with energy (See Fig.10) so that this equation is expected to hold quite accurately, even for relatively large ΔE values. The value of the stopping power for ^{1}H at 60 KeV can be found using Eq.(III.B.1) and the results in Fig.10. Eq.(V.A.1) then yields

(V.A.2) $$D = 65 \Delta E$$

where ΔE is expressed in KeV and D in A^{o}.

B. The Deterioration Depth of ^{4}He, ^{14}N, ^{40}Ar and ^{129}Xe

Fig.15 is a plot of the energy loss of ^{1}H, at 60 KeV, versus the irradiation dose for xenon. The three curves are for different

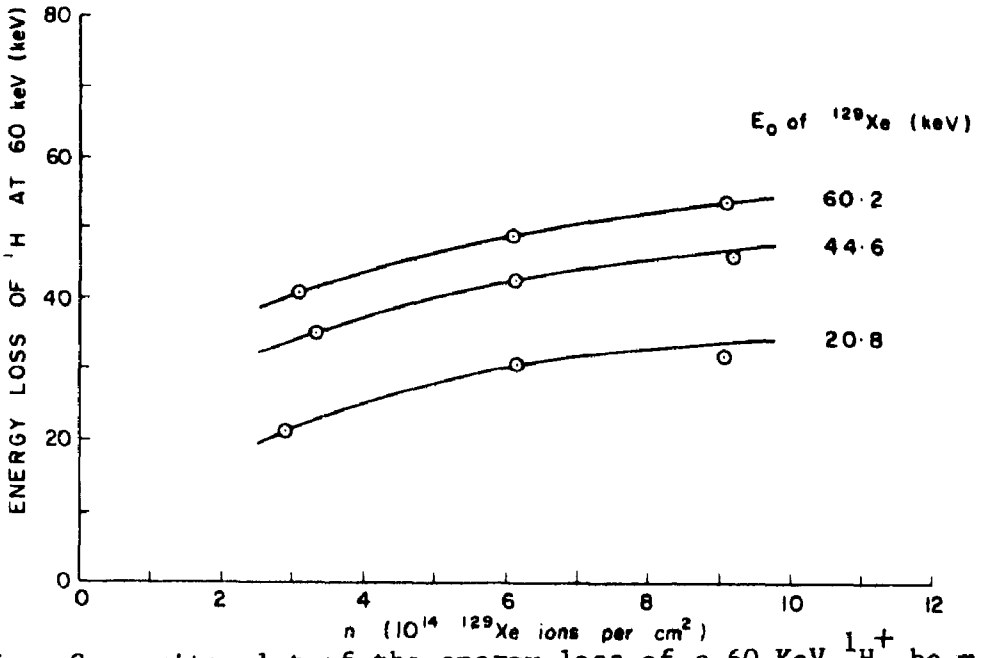

Fig. 15. Composite plot of the energy loss of a 60 KeV $^{1}H^{+}$ be m in traversing phosphor regions damaged by $^{129}Xe^{+}$ ions, versus, n, the number of these damaging projectiles per cm^2, for various bombarding energies, E_o.

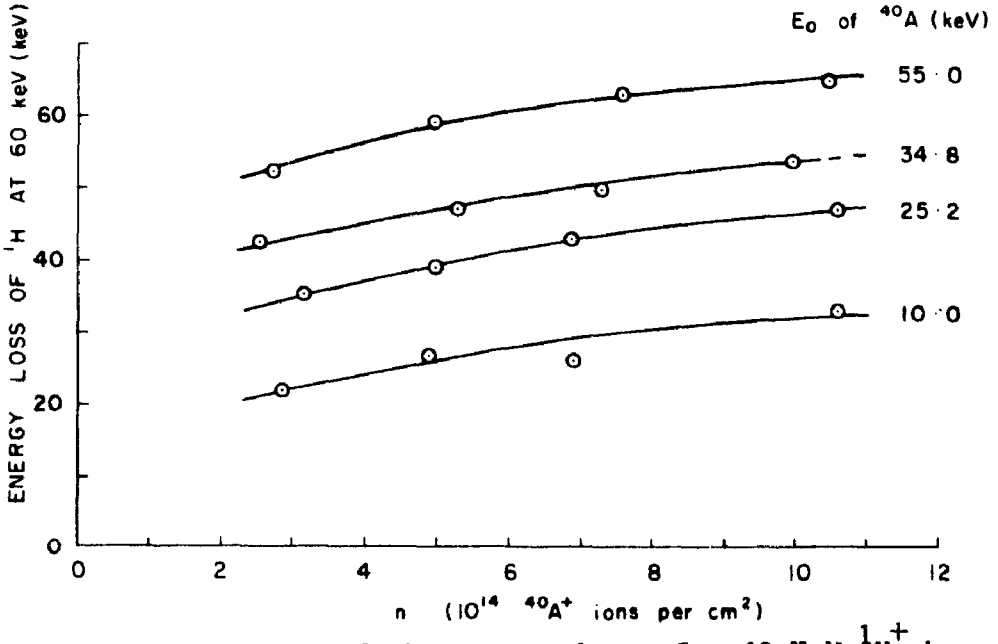

Fig. 16. Composite plot of the energy loss of a 60 KeV $^{1}H^{+}$ beam in traversing phosphor regions damaged by $^{40}Ar^{+}$ ions, versus n, the number of these damaging ions per cm^2, for various bombarding energies E_o.

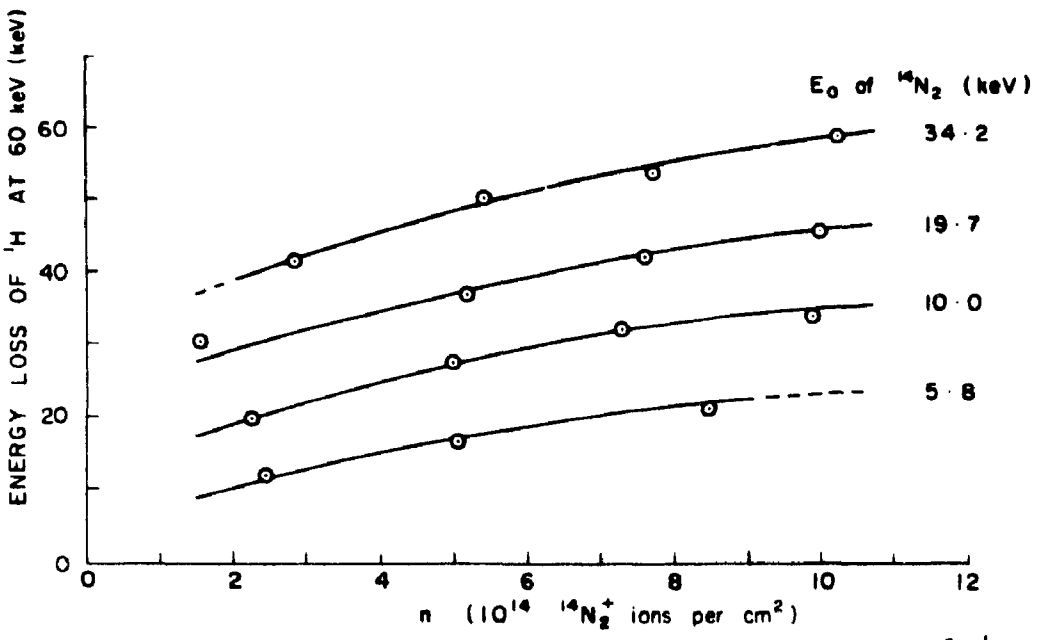

Fig. 17. Composite plot of the energy loss of a 60 KeV $^1H^+$ beam in traversing phosphor regions damaged by $^{14}N_2^+$ ions, versus n, the number of these damaging projectiles per cm^2, for various bombarding energies, E_0.

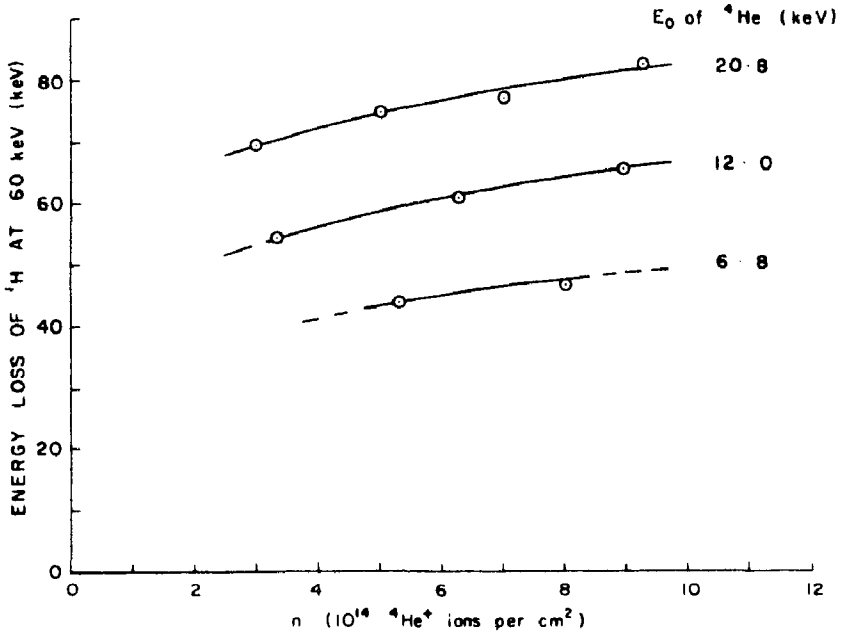

Fig. 18. Composite plot of the energy loss of a 60 KeV $^1H^+$ beam in traversing phosphor regions damaged by $^4He^+$ ions, versus n, the number of these damaging projectiles per cm^2, for various bombarding energies, E_0.

incident Xe energies as shown in the figure. Figs. 16, 17 and 18 present the ΔE measurements for hydrogen after a phosphor sample was deteriorated by argon, nitrogen and xenon at the energies indicated in the figures.

It was observed that the measured energy loss of hydrogen, was only reproducable [see (II.)] to within about $\pm$ 10 percent . This accounts almost entirely for the scatter in the experimental points.

It will be noted from the figures that the energy loss of hydrogen, and thus the deterioration depth, increases with n. Thus it is difficult to form criteria for the comparison of the deterioration depths, of the various projectiles. Since, however, the depths do not vary rapidly with the irradiation dose, it seems reasonable to compare the depths for the different projectiles at a fixed value of n. Fig. 19 is a plot of the deterioration depth versus the square root of the deterioration energy, E_o. The circles, triangles, crosses and squares correspond

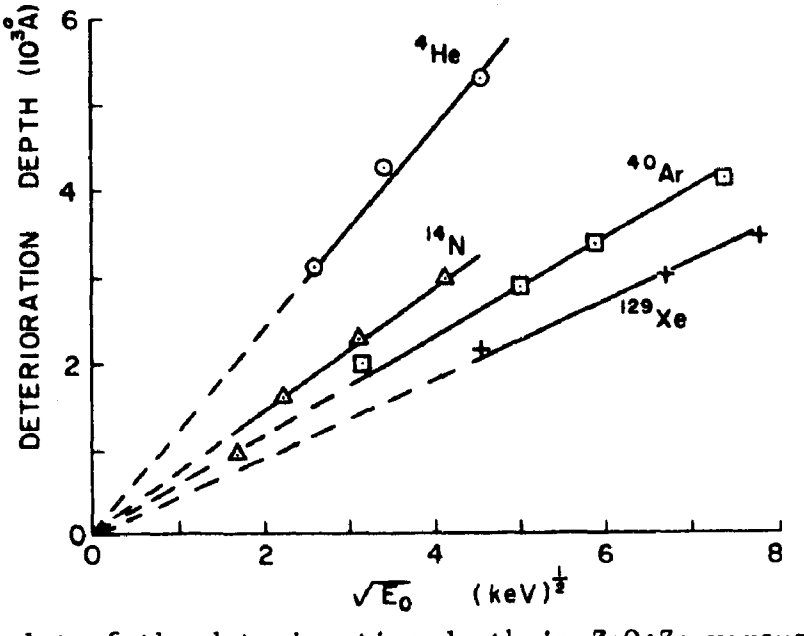

Fig. 19. A plot of the deterioration depth in ZnO:Zn versus the square root of the deterioration energy. (see text). The circles, triangles, squares and crosses present D values, for a common n value of 8×10^{14}, for ^{4}He, ^{14}N, ^{40}Ar and ^{129}Xe, respectively.

to He, N, Ar and Xe, respectively. The ΔE values for ^{1}H (at 60 KeV) were read from Figs. 15 - 18 for a common irradiation dose of 8×10^{14} atomic projectiles per cm^2 and the corresponding D values were computed by means of Eq. (V. A. 2). A D value for ^{14}N at an energy E_o and with an irradiation dose of 8×10^{14} $^{14}N^+$ cm^{-2} was assumed to be equivalent to an observed D value for $^{14}N_2^+$ at an energy $2\ E_o$ and with an irradiation dose of 4×10^{14} N_2^+ cm^{-2}. In Fig. 19 straight lines have been drawn through the points which, within experimental error, intersect the origin, showing that the deterioration depth is proportional to the velocity.

C. Discussion

The observed deterioration depths, for the heavier projectiles, are much larger than the average ranges wich may be obtained from a consideration of the average energy loss (see section III.B). The reason for such a behavior may be qualitatively understood in the following manner.

When a projectile slows down in a stopping material it loses energy through electronic collisions in which the particle is but little deflected and by nuclear collisions in which violent scattering events may occur. The variation in the energy loss per nuclear collision is much larger than that per electronic collision. Thus heavy projectiles, for which nuclear energy loss dominates, exhibit considerable straggling in their ranges. If a particular projectile, in traversing a stopping material, suffers only small energy losses in nuclear collisions, then its trajectory will be almost straight, and its range determined to a considerable extent by the energy it loses through electronic collisions. If a range R_e is defined, which is

given by,

$$(V.\ C.\ 1) \qquad R_e = \int_o^{E_o} (dE / dR)_e^{-1}\, dE,$$

then this range should be a measure of the maximum distance a projectile may travel in a stopping medium.

Although only a small percentage of the projectiles incident on a phosphor sample will have ranges comparable to R_e, the deterioration may extend this far below the surface, for large irradiation doses. Thus the deterioration depth may be a measure of the maximum range.

Integration of the above equation, using the theoretical stopping powers (see section I. A.) yields an $E_o^{1/2}$ dependence for R_e. It will be noted from Fig. 19 that the deterioration depths also have such an energy dependence. Table V compares the observed deterioration depths, D, to the theoretical maximum range, R_e, for the various projectiles, at incident energies of 16 KeV.

TABLE V

Comparison of D and R_e at 16 KeV.

Projectile	$D(10^3\ A^o)$	$R_e(10^3\ A^o)$	R_e / D
^4He	4.75	3.46	1.37
^{14}N	2.90	2.12	1.37
^{40}Ar	2.30	1.73	1.34
^{129}Xe	1.80	1.62	1.10

The deterioration depths, listed in the second column, are about 30 per cent larger than the predicted maximum ranges, listed in the third column. Such a discrepancy lies well within the theoretical limits of R_e [see (I. A)] and the uncertainty in the accuracy with which D was determined. It may be added that in a similar experiment using ZnS:Ag (van Wijngaarden and Hastings 1967), in which n values an order of magnitude smaller could be used, D's were obtained that differed by less than 5 per cent from R_e.

Although this correspondance is quite convincing the concept of an electronic range can be criticized. Since the stopping medium is crystalline, channelling may occur and the electronic stopping cross section may be reduced in magnitude. One, however, would not expect the electronic stopping cross section to be reduced by such channelling to the same extent as the nuclear stopping cross section. The phosphor samples used in this experiment consisted of tiny randomly oriented crystals thus it is hard to see how channelling could have influenced our results to a significant degree.

CHAPTER VI

THE DETERIORATION CONSTANT

A. The Decrease In Light Output Under Continuous Bombardment

When a phosphor sample is subjected to continuous ion bombardment the light output decreases in time as shown in Fig. 20. The figure is a plot of the relative light output, L / L_o, versus the irradiation dose, n, for ^{14}N, ^{4}He, and ^{40}Ar each with an incident energy of 15 and 60 KeV, and for ^{1}H at 60 KeV. A study of the figure reveals some interesting effects. At 60 KeV the rate of deterioration increases with projectile mass, whereas at 15 KeV ^{14}N damages the phosphor more effectively than ^{40}A. For the more massive projectiles the rate of deterioration increases with increasing projectile energy, while for helium the reverse is true. Thus the deterioration of ZnO:Zn is energy dependent. This energy dependence will be discussed in further detail in Section E.

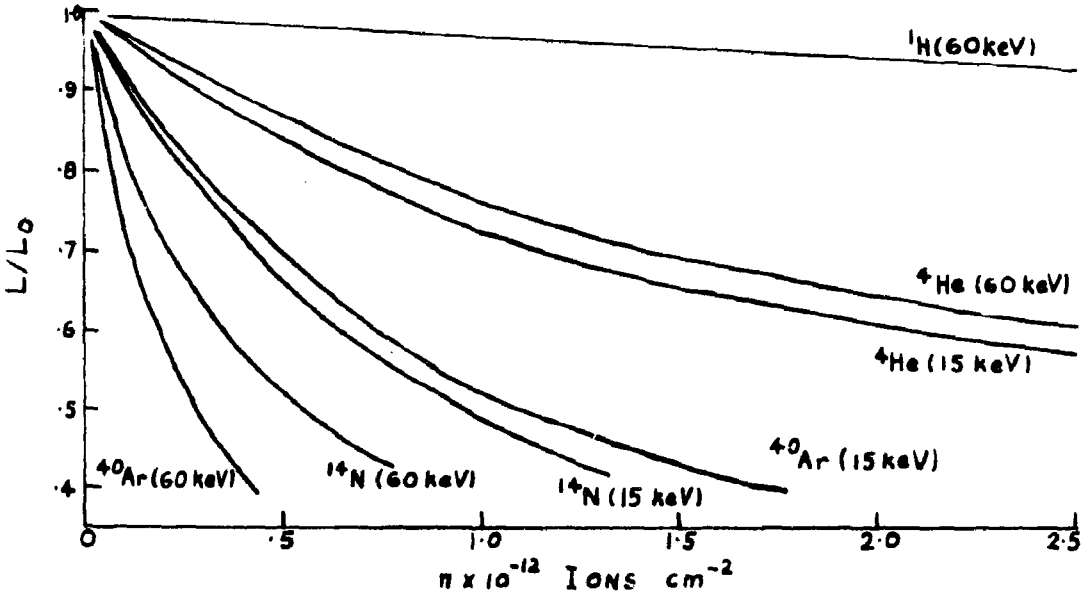

Fig. 20. A plot of the relative light output, L / L_o, during irradiation, versus the irradiation dose, n, for ^{1}H, ^{4}He, ^{14}N and ^{40}Ar. The energies are incident energies.

B. The Surface Damage of ZnS:Ag

When the efficiency of a phosphor is determined by the light produced during irradiation, the surface plays a significant role. It is near the surface that an ion has its maximum energy and produces most of the observed light. If after prolonged bombardment, the surface of the phosphor differs from the bulk of the damaged material just below it, the deterioration constants obtained by Hanle and Rau will not be representative of the phosphor and will be of questionable significance.

Since Hanle and Rau found Eq. (I. C. 1) to hold most accurately for ZnS:Ag, the surface properties of this phosphor were first investigated. A sample of ZnS:Ag (Sylvania Type 130) was deteriorated, with the exit slit fully open, by 1×10^{12} H_2^+ cm^{-2} at various energies. The corresponding L / L_o values after deterioration are listed in the second column of Table VI. To determine the properties of the damaged phosphor near the surface, the exit slit was reduced in size and the sample scanned with 10 KeV $^{40}Ar^+$ ions, whose penetration depth is an order of magnitude less than that of hydrogen. The light outputs thus observed are representative of the efficiencies of the surface layers, and the corresponding L / L_o values have been equated to the relative surface efficiencies, η / η_o, listed in the last column of the table.

TABLE VI

A Qualitative Comparison of the Surface Efficiency to that of the Bulk of the Damaged Phosphor Immediately Below it.

Deterioration Energy (KeV)	L / L_o	η / η_o
100	.85	.48
75	.77	.43
50	.74	.31
25	.67	.22

It will be noted from the table that the zincsulphide phosphor deteriorated much more rapidly near the surface than in the bulk of the material. Thus neither L / L_o nor η / η_o are true measures of the average damage in the bulk of the phosphor. The table also shows that the deterioration depends upon the energy of the damaging projectiles.

C. The Distribution of Damage in ZnO:Zn

In this set of experiments the surface properties of damaged ZnO:Zn were investigated. A phosphor sample was deteriorated in two local regions, with 2.62×10^{12} and 7.25×10^{12} $^4He^+$ cm^{-2}, at 102 KeV, with the exit slit fully open. At this energy S_n for helium varies fairly rapidly (See Fig. 12) with energy. In the first 10^3 A^o of its range we find, from Fig. 11, that the energy of the He^+ ion changes from 102 KeV to about 75 KeV and in this energy interval S_n changes from 1.4×10^{-15} - 1.6×10^{-15} eV-cm^2. Thus in this distance S_n only changes by about 15 per cent and consequently the variation in the degree of damage is also expected (see Eq. I. C. 16) to be small (not more than 15 per cent) provided the surface deteriorates at the same rate as the phosphor immediately below it. After it had been damaged the sample was scanned with $^4He^+$ ions at various energies and the light output, L_1, for damaged phosphor and that, L_o, for undamaged phosphor were observed. Fig. 21a is a plot of L_1/L_o versus energy, with (crosses) and without (circles) the green filter in position. It will be noted that L_1/L_o, corresponding to a given irradiation dose, is almost independent of energy. This indicates that the deterioration was fairly uniform over an appreciable volume of the damaged phosphor. The relative efficiencies of the phosphor regions damaged by 2.62×10^{12} and 7.25×10^{12} $^4He^+ cm^{-2}$, are about .65

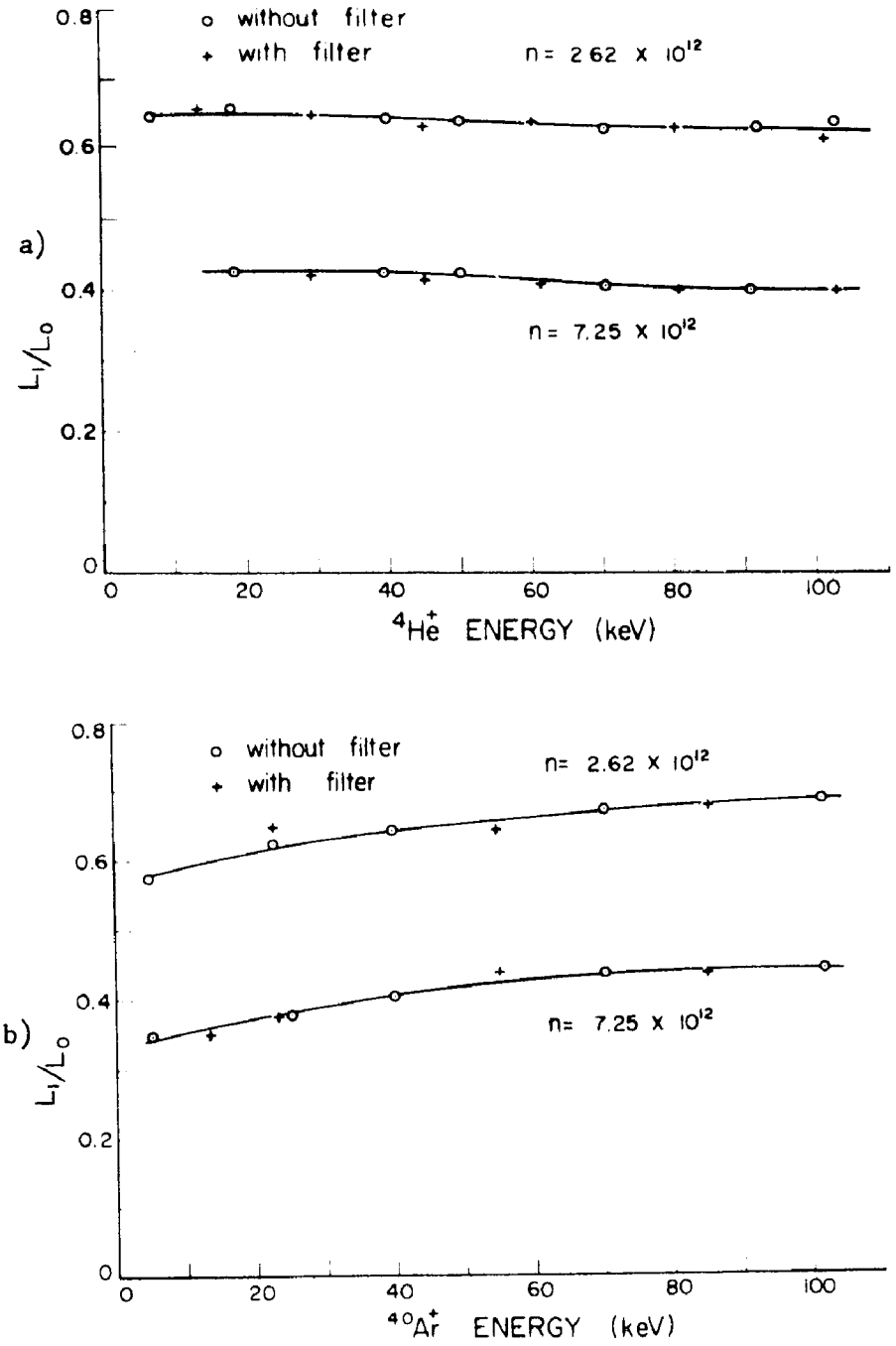

Fig. 21. a) A plot of the ratio L_1 / L_o of the light produced in damaged phosphor to that produced in undamaged phosphor versus the incident energy of a $^4He^+$ beam. The upper and lower curves correspond to phosphor damaged by 102 KeV $^4He^+$ with irradiation dose of 2.62×10^{12} and 7.25×10^{12} ions cm^{-2}, respectively. The crosses and circles are observed light outputs obtained with and without a filter in position, respectively. b) A plot similar to (a) for the sample scanned with $^{40}Ar^+$.

and .42 respectively.

To investigate the surface properties of the damaged phosphor the same sample was scanned with ^{40}Ar, for which the penetration depth is an order of magnitude less than that for ^{4}He. Fig. 21 b is a plot, similar to Fig. 21a, of the L_1 / L_o values obtained from the argon scans. At lower argon energies the relative efficiencies of the two damaged regions are .6 and .35, approximately 10 percent less than those found for the bulk of the damaged material from the helium scan. Since at low energy the light L_1, produced by argon, comes from a very thin layer of phosphor at the surface, these observations were taken to indicate that the surface of deteriorated ZnO:Zn has approximately the same properties as the damaged material below it. This may be contrasted to the observations made with the zinc sulphide phosphor, where the damage at the surface of the sample was greater by more than 100 percent than that in the bulk of the material.

Figures 21a and 21b, also indicate that the ratio, L_1/L_o, is independent, within experimental error, of whether the light was observed through a filter or allowed to fall on the photomultiplier tube directly. This was taken to indicate that the spectral distribution in the light produced by ZnO:Zn did not change as a result of deterioration.

The observed nuclear stopping cross section, S_n, for the heavier projectiles, decreases quite rapidly with decreasing projectile energy (see section II. D.). Thus the damage caused by the heavier projectiles is expected to decrease with increasing depth below the phosphor surface. (see Eq. I. C. 6) This effect is shown in Fig. 22,

which presents L_1 / L_o values for a sample deteriorated at 102 KeV with 2.5×10^{11} $^{40}Ar^+$ cm^{-2}, and scanned with argon ions at various energies. The relatively large slopes of the curves indicate that the damage is non-uniform and increases as the surface of the phosphor is approached.

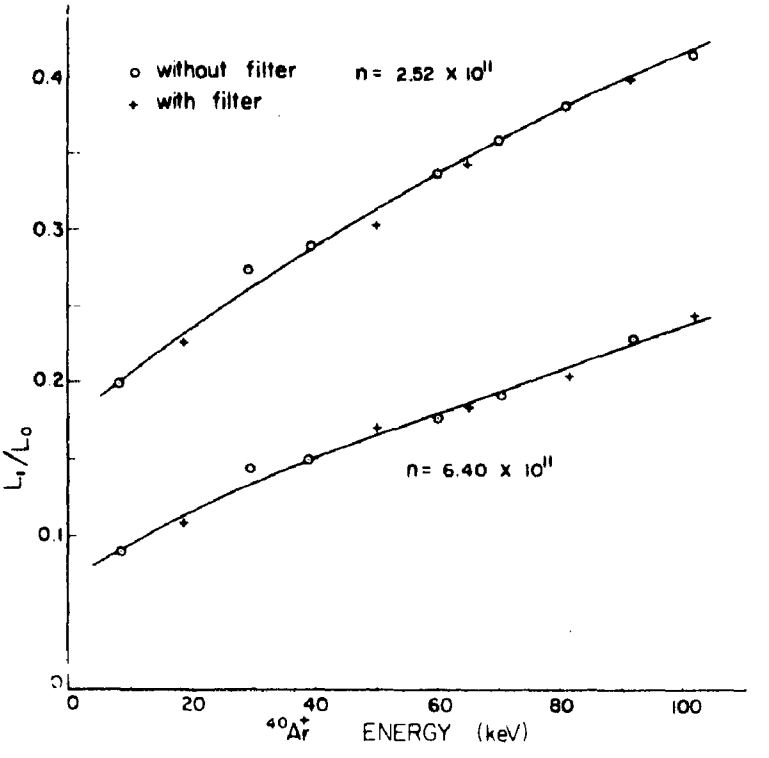

Fig. 22. A plot of the ratio L_1 / L_o for a sample deteriorated in two regions with 2.52×10^{11} and 6.40×10^{11} $^{40}A^+$ cm^{-2} at 102 KeV, versus incident $^{40}Ar^+$ energy. Crosses and circles are experimental points with and without the filter in position respectively.

D. Technique For the Measurement of Deterioration Constants.

When a ZnO:Zn phosphor is deteriorated with energetic projectiles a thin layer at the surface, in which the energy loss of the projectile is small, will be almost uniformly damaged. The deterioration constant for a particular projectile is related to the surface efficiency, η, as

(I. C. 7) $$C(E) = (\eta_o / \eta - 1)n^{-1} ,$$

where η_o is the surface efficiency of undetericrated phosphor and E is the incident energy of the damaging projectiles. The surface efficiencies can be measured by observing the light outputs as the damaged phosphor is scanned across beams of low energy ions, whose penetration depths are relatively small. In the following experiments phosphors were deteriorated by energetic ions until the light output was reduced by 80-30 percent and then the surface efficiencies were measured with 5 KeV $^{40}Ar^+$ ions.

E. The Deterioration Constant For ^4He

Several local regions of a ZnO:Zn phosphor sample were irradiated, with the exit slit fully open, by 2 x 10^{12} $^4He^+$ cm^{-2}, each at a different energy in the range 3 - 100 KeV. The exit slit was then reduced in size and the sample was rapidly scanned across beams of 5 KeV argon ions, whose currents were kept small to prevent further deterioration of the phosphor. The experiment was thenrepeated on a new sample with an irradiation dose of 1 x 10^{12} $^4He^+$ cm^{-2}.

Fig. 23 is a plot of C versus the incident energy of helium used to produce the varius damaged regions. The circles and crosses correspond to irradiation doses of 2 x 10^{12} $^4He^+$ cm^{-2} and 1 x 10^{12} $^4He^+$ cm^{-2}, respectively. The two curves in the figure differ by only a few per cent whereas the irradiation doses to which they correspond differ by a factor of two. thus it appears that Eq.(I.C.6) holds with a fairly high degree of accuracy. The discrepancy between the two curves will be further discussed in the next section.

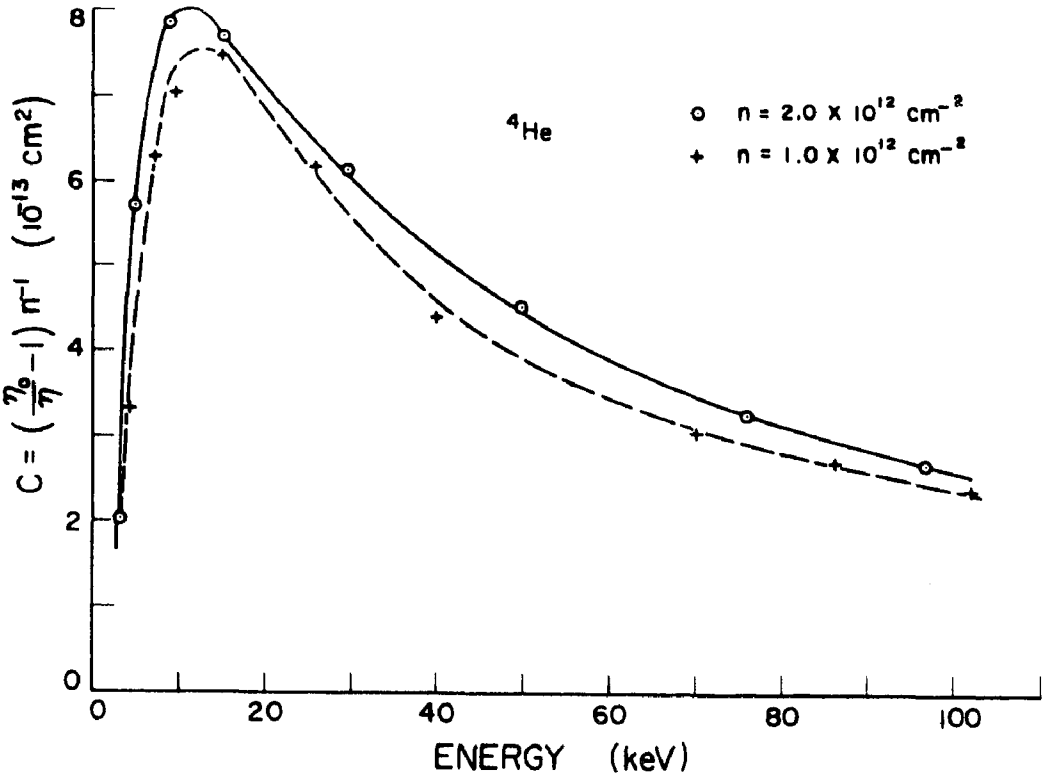

Fig. 23. The deterioration constant of ZnO:Zn for $^4He^+$ ions versus energy. The circles and crosses correspond to irradiation doses of 2.0×10^{12} and 1.0×10^{12} $^4He^+$ cm^{-2}, respectively.

F. The Deterioration Constants for ^{40}Ar and ^{14}N

Fig. 24a. is a plot of the observed deterioration constants versus energy for ^{40}Ar. The circles and crosses correspond to irradiation doses of 5×10^{11} and 2.5×10^{11} $^{40}Ar^+$ ions cm^{-2}, respectively, and were obtained with different phosphor samples. The circles and crosses in Fig. 24b. correspond to C values obtained with the same irradiation doses as those in Fig. 24a. on a single sample. It will be noted that the C values obtained for different irradiation doses on different samples differ on the average by about 20 percent whereas those obtained on the same sample are much more nearly the same. Thus the observed C values depend to some extent upon the sample and are not quite reproducable. Because of this, the results in a particular

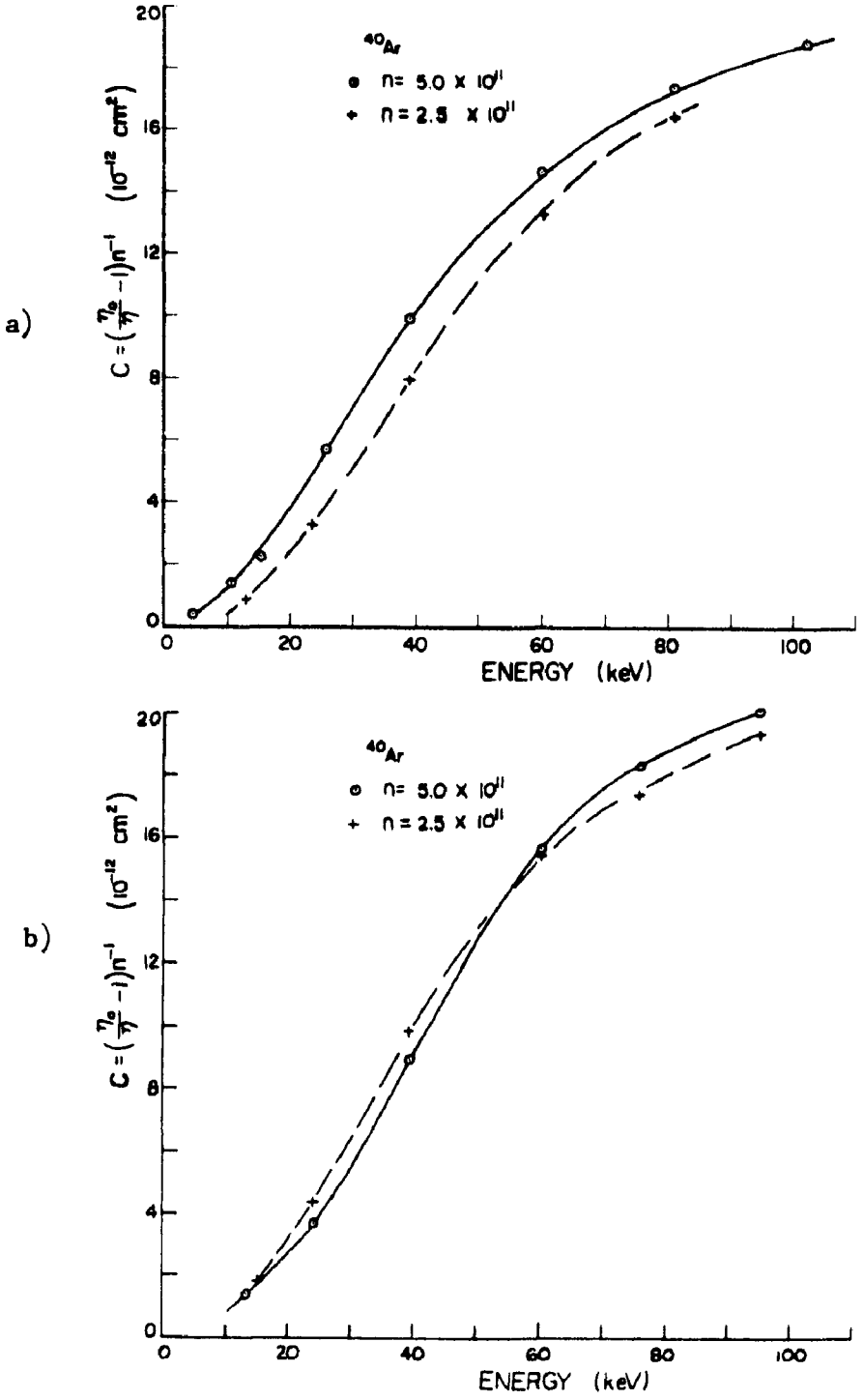

Fig. 24. a) and b) are similar plots of the deterioration constant of ZnO:Zn for $^{40}Ar^+$, versus energy. The circles and crosses correspond to irradiation doses of 5.0×10^{11} $^{40}Ar^+$ cm^{-2}, respectively. The curves in a) were obtained from different phosphor samples, whereas those in b) were obtained from the same sample.

C - E plot can only be referred to as typical. Part of the irreproducibility may be associated with a possible variation in the average size of the phosphor particles at the surface which may have varied from sample to sample [see (II)].

At low energies the curves in Fig. 24a are separated by a few KeV, indicating the presence of a dirt layer on the surface of the phosphor samples. The thickness of the layer probably depends upon the exact method of preparation of the phosphor sample, which may also at least in part, explain the variation of the C values for different samples. Since for ^{40}Ar the energy loss in the dirt layer may be perhaps as large as 10 KeV, the C values below about 20 KeV are quite uncertain. The observed C values for heavier projectiles should even be more uncertain and are, therefore, not presented in this thesis.

Fig. 25 is a typical plot of the C value versus energy for ^{14}N. The curve was obtained for an irradiation dose of 1×10^{12} ions cm^{-2} and will be further discussed in (VI.H.).

G. The Deterioration Constant for ^{1}H

In order to obtain a sufficiently large irradiation dose to deteriorate the phosphor to a significant degree it was necessary to use molecular hydrogen ions with which a much larger beam current was available than with protons. The deterioration constant for ^{1}H, however, can be obtained from observations made with an $^{1}H_2$ beam by dividing the deterioration energy of the latter by 2 and multiplying the irradiation dose by the same factor. To check the validity of this procedure for determining C for ^{1}H, samples of ZnO:Zn and ZnS:Ag were

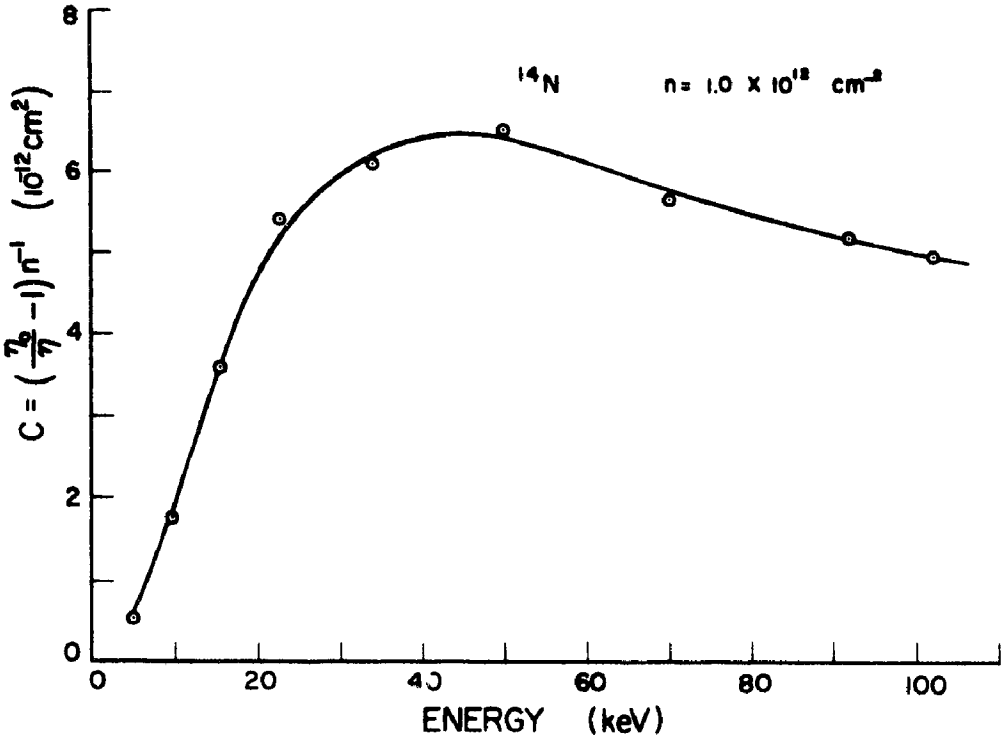

Fig. 25. A typical plot of the deterioration constant of ZnO:Zn for $^{14}N^+$ versus energy for an irradiation dose of 1.0 x 10^{12} ^{14}N cm^{-2}.

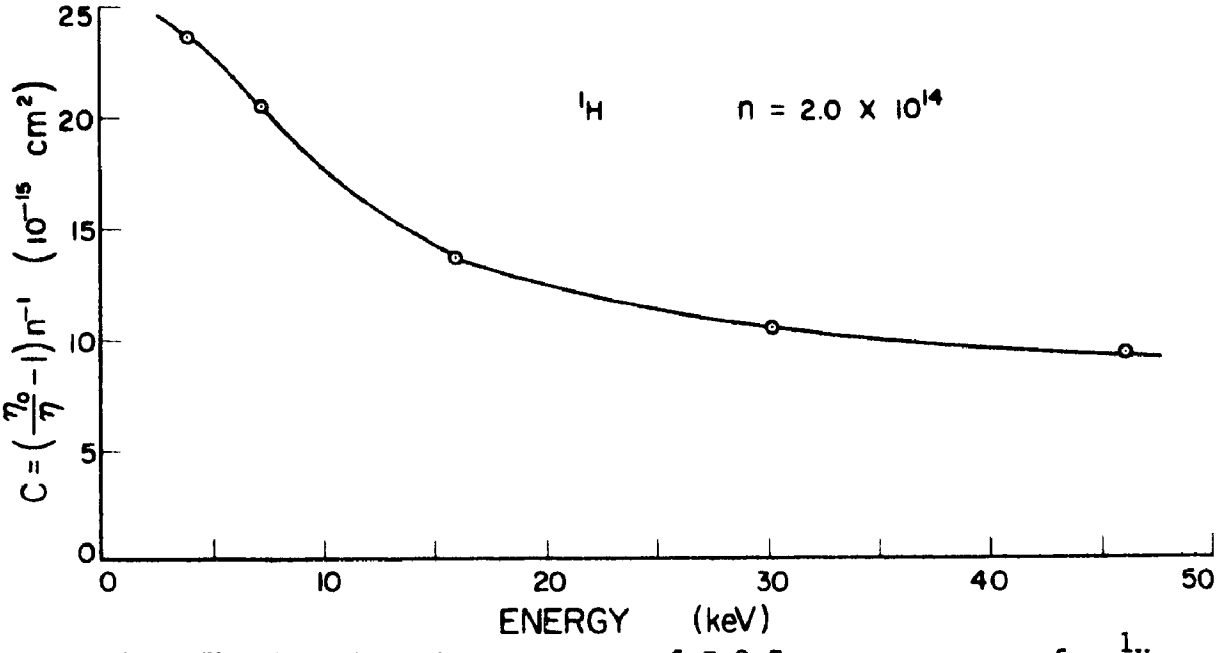

Fig. 26. The deterioration constant of ZnO:Zn versus energy for ^{1}H. (see text.)

deteriorated with atomic and molecular hydrogen, with only small irradiation doses. It was found that the rate of deterioration of both phosphors with ^{1}H could be predicted within experimental error ($\pm$ 7 percent) from that of $^{1}H_2$.

Fig. 26 is a typical plot of the C value versus energy for ^{1}H. The different regions on the sample were irradiated by 1×10^{14} $^{1}H_2^{+}$ cm^{-2} and consequently the n value in the figure is twice as large.

H. Discussion

Typical results for the C values of H, He, N and Ar are summarized in Fig. 27. This figure is a composite diagram showing logarithmic plots of S_n and C versus energy for various projectiles. The solid curves are the nuclear stopping cross sections for ^{40}Ar and ^{14}N, obtained from Fig. 12. The dashed curves are the theoretical nuclear stopping cross sections for ^{1}H and ^{4}He and the stippled dashed curves are the C values for the various projectiles. The left ordinate indicates the magnitude of S_n and the right that of C. Since the magnitude of the proportionality constant [see Eq. (I. C. 16)] relating S_n to C is not known, these ordinates were adjusted for the best fit of the C values to the corresponding S_n values for the heavier projectiles. The figure indicates good agreement between the relative magnitudes of the S_n and C curves for Ar, N and He at higher energies. At lower energy the deterioration constant for ^{40}A and ^{14}N decreases slightly more rapidly with decreasing energy than does the nuclear stopping cross section. This may be due to the

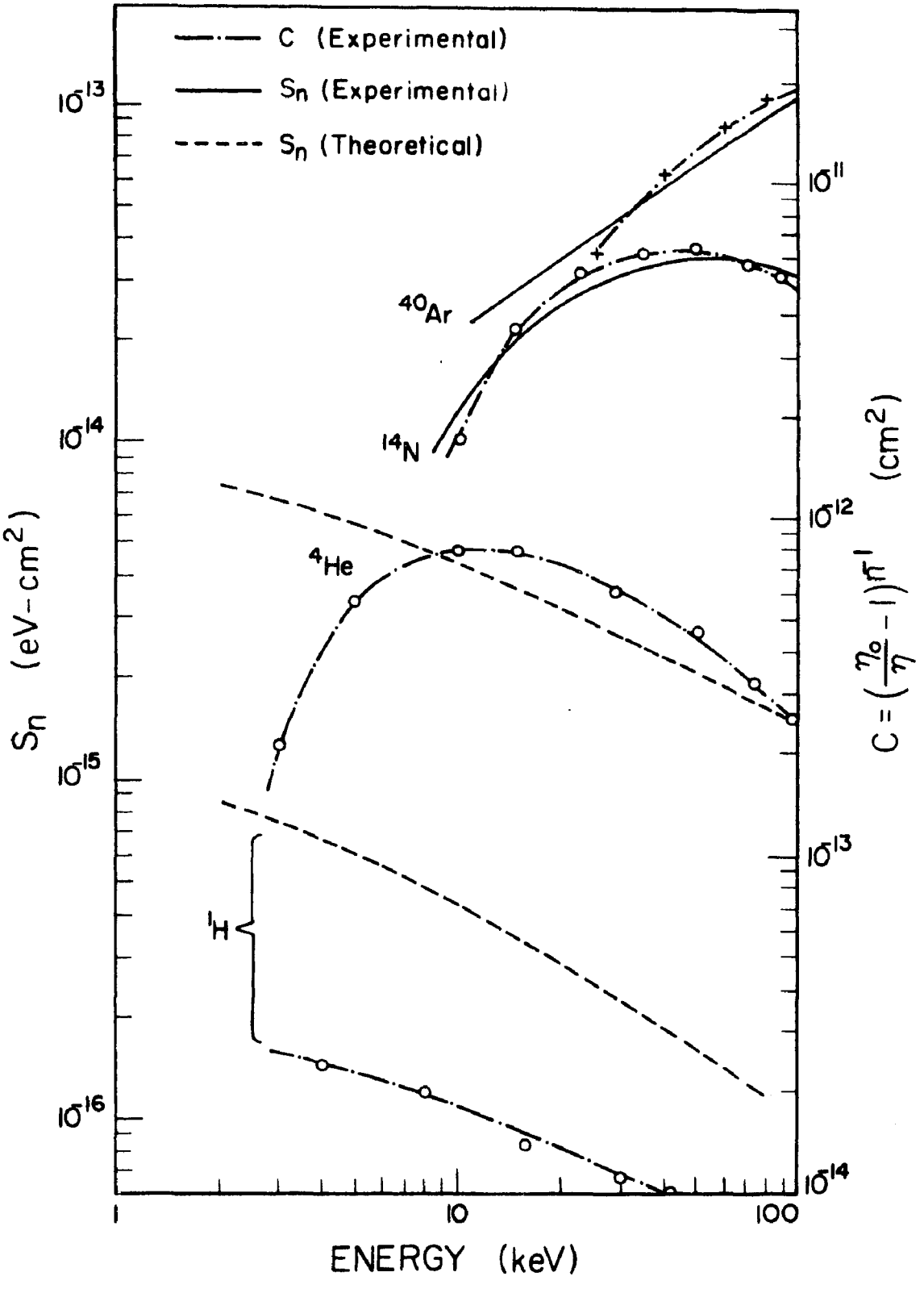

Fig. 27. Composite diagram showing logarithmic plots of the nuclear stopping cross section, S_n, and the deterioration constant C both as a function of energy. Points are observed values of the deterioration constant. The nuclear energy loss cross sections are replotted from Fig. 12, without showing experimental points for ^{14}N and ^{40}A.

presence of thin dirt layers which would tend to shift the lower energy C values to higher energies.

The deterioration constant for hydrogen is about a factor of 3 lower than S_n, relative to the other projectiles. The simplified calculation of C in (I. C.) indicated that it should be lower but the magnitude of the discrepancy seems rather large. It should be emphasized, however, that the nuclear energy loss curves for ^{1}H and ^{4}He were not experimentally determined, and a comparison between them and the corresponding C values may not be meaningful.

CHAPTER VII

CONCLUSION

A. Energy Loss

The total average energy loses of several projectiles in traversing thin films of ZnO:Zn, consisting of tiny randomly oriented crystals, were measured. At low projectile velocities the relative magnitudes of the energy losses, for the heavier projectiles were found to be much lower than the theoretically predicted ones. This discrepancy may be due to the fact that the stopping medium was crystalline, and thus the effective average nuclear energy loss is lower than the predicted one as a result of channeling or some related effect. This conclusion is in qualitative agreement with Lutz et al(1965) who stated, "Integral range distribution measurements performed on crystalline substances, and theoretical range energy relations calculated from a random lattice cannot be compared."

B. Light Output

The distribution in the luminescent spectrum of ZnO:Zn exhibits two peaks, which may be associated with different excited states of the crystal (Heiland et al 1959). One might expect the number of electrons excited to each of these states to vary with projectile energy and mass. In the energy range studied no significant effects of this nature were observed.

The light output of the phosphor was found to be proportional to the total amount of energy lost to the target atoms.

The proportionality constant, however, varied with the projectile mass.

C. Deterioration Depth

The depth of deterioration, D, was found to correspond quite closely to a range, R_e, which is determined by the electronic stopping power. Thus after prolonged bombardment the phosphor is deteriorated to a depth which approximately equals the maximum range of the damaging projectiles.

D. Deterioration Constant

The deterioration constant, C(E), is a measure of the ability of an ion, at an energy E, to deteriorate a phosphor. Above about 10 KeV the relative magnitudes of the deterioration constants for ZnO:Zn were found to agree quite closely to the corresponding nuclear stopping cross sections, for ^{4}He, ^{14}N and ^{40}Ar, in agreement with the form of Eq. (I. C. 16). Since S_n changes by almost 3 orders of magnitude in this mass range such a correspondence is more than coincidental, and we conclude that the radiation damage in phosphors by heavy ions is now fairly well understood.

APPENDIX I

The Nuclear Energy Loss and Displacement Cross Sections

To obtain the nuclear stopping cross section, S_n, Lindhard et al. (1963) considered scattering to take place in the potential,

(A. I. 1) $$U(r) = \frac{Z_1 Z_2 e^2}{r} \varphi_o (r / a),$$

where φ_o is the Fermi function and a is the screening parameter given by Eq. (I. A. 5). This potential differs from the screened coulomb potential discussed in (I. A) in that it falls off less rapidly at large distances r. With such a potential the variables ρ and ϵ [see Eq. (I. A. 4)] are natural measures of the range R and energy E respectively.

The differential crossection for the transfer of kinetic energy T to a target atom by a projectile with energy E is given by,

(A. I. 2) $$d\sigma (E, T) = \frac{\pi a^2 f(t^{1/2})}{2 t^{3/2}} dt ,$$

where $t = \epsilon^2 T / T_m$ and

$f(t^{1/2}) = (\pi a^2)^{-1} 2 t^{3/2} (d\sigma / dt)$ is a universal function valid for all projectiles and stopping atoms. Fig. 28. is a reproduction of $f(t^{1/2})$ versus $t^{1/2}$ from Lindhard et al. (1963).

The average energy loss per collision, taking into account all possible energy transfers (the nuclear stopping crossection) is given by,

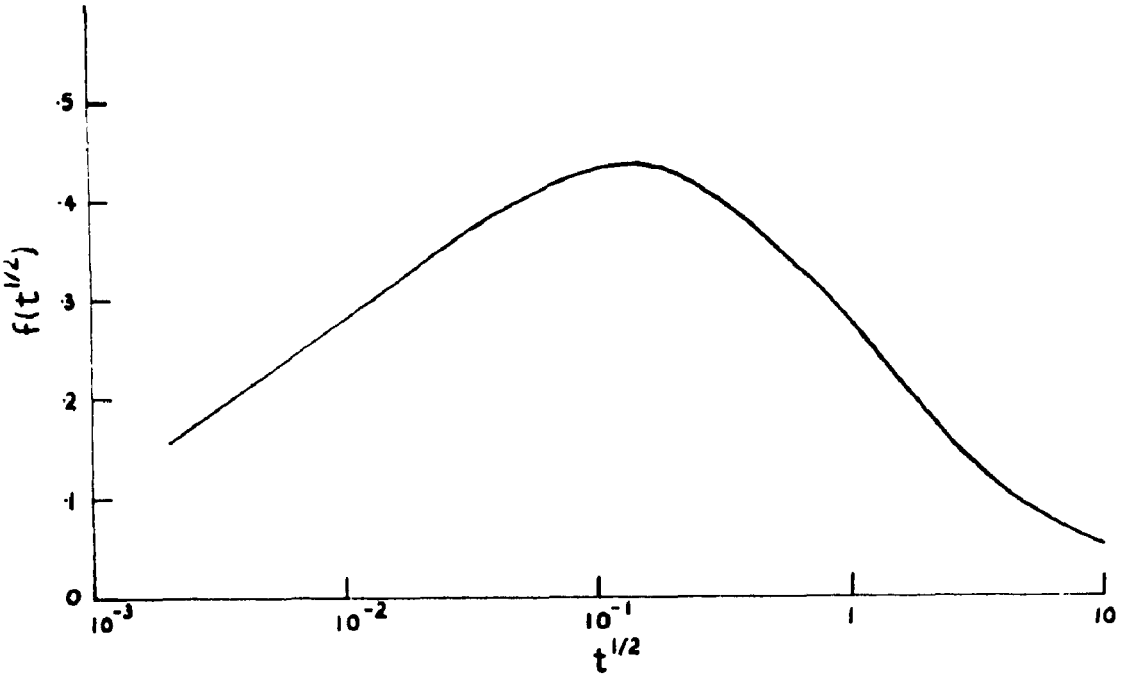

Fig. 28 A plot of $f(t^{1/2})$ versus $t^{1/2}$ (from Lindhard et al. 1963)

(I. C. 13) $$S_n(E) = \int_0^{Tm} T\, d\sigma(ET).$$

This equation may be written [see Eq. (A. I. 2)] in terms of the variables t and ϵ as,

(A. I. 3) $$S_n(\epsilon) = 4\pi a \frac{M_1}{M_1 + M_2} Z_1 Z_2 \epsilon^2 \int_0^{\epsilon} \epsilon^{-1} f(t^{1/2}) d(t^{1/2})$$

The integral can be obtained by numerical integration, and its value when plotted against $\epsilon^{1/2}$ is the universal curve for $(d\epsilon / d\rho)_n$ in Fig. 1.

The average number of displacements resulting from a single collision (the displacement crossection) is given by,

(I. C. 10) $$\sigma_d(E) = \int_0^{T_m} \nu(T)\, d\sigma(E, T)$$

where $\nu(T)$, the number of displacements introduced when the incident projectile transfers an energy T to a target atom, is given by Eq. (I. C. 9). Substitution of Equation (I. C. 9) and (A. I. 2) into

Eq. (I. C. 10) and using Equations (A. I. 3) and (I. A. 4) yields

$$\text{(A. I. 4.)} \qquad \sigma_d(E) = \pi a^2 \int_{\epsilon\sqrt{E_d/T_m}}^{\epsilon\sqrt{2E_d/T_m}} t^{-1} f(t^{1/2})\, d(t^{1/2}) + \frac{4\pi a}{2E_d} Z_1 Z_2 e^2 \int_{\epsilon\sqrt{2E_d/T_m}}^{\epsilon} \epsilon^{-1} f(t^{1/2})\, d(t^{1/2})$$

This equation is, strictly speaking only valid for a stopping medium which consists of a single atomic species. The work presented in this dissertation employs a ZnO:Zr stopping medium which is diatomic. In order to make a comparison between σd and $S_n / 2Ed$ in a montomic stopping medium, Z_2 and M_2 were taken to be 19 and 42 respectively, the average value of these quantities for Zn and O. The values of σd and $S_n / 2\,Ed$ were then obtained by numerical integration of Equations (A. I. 3) and (A. I. 4) using Fig. 28 and an Ed value of 25 eV. The results of these computations are summarized in Fig. 29 which is a logarithmic plot of σ d and $S_n / 2$ Ed versus energy for various projectiles. It will be noted that for ^{40}Ar and ^{84}Kr

$\sigma_d \simeq \frac{S_n}{2Ed}$ while for the lighter projectiles $\sigma_d < \frac{S_n}{2Ed}$,

indicating that these projectiles may suffer a large number of small angular deflections in which the transfer of energy is not sufficient to cause displacements.

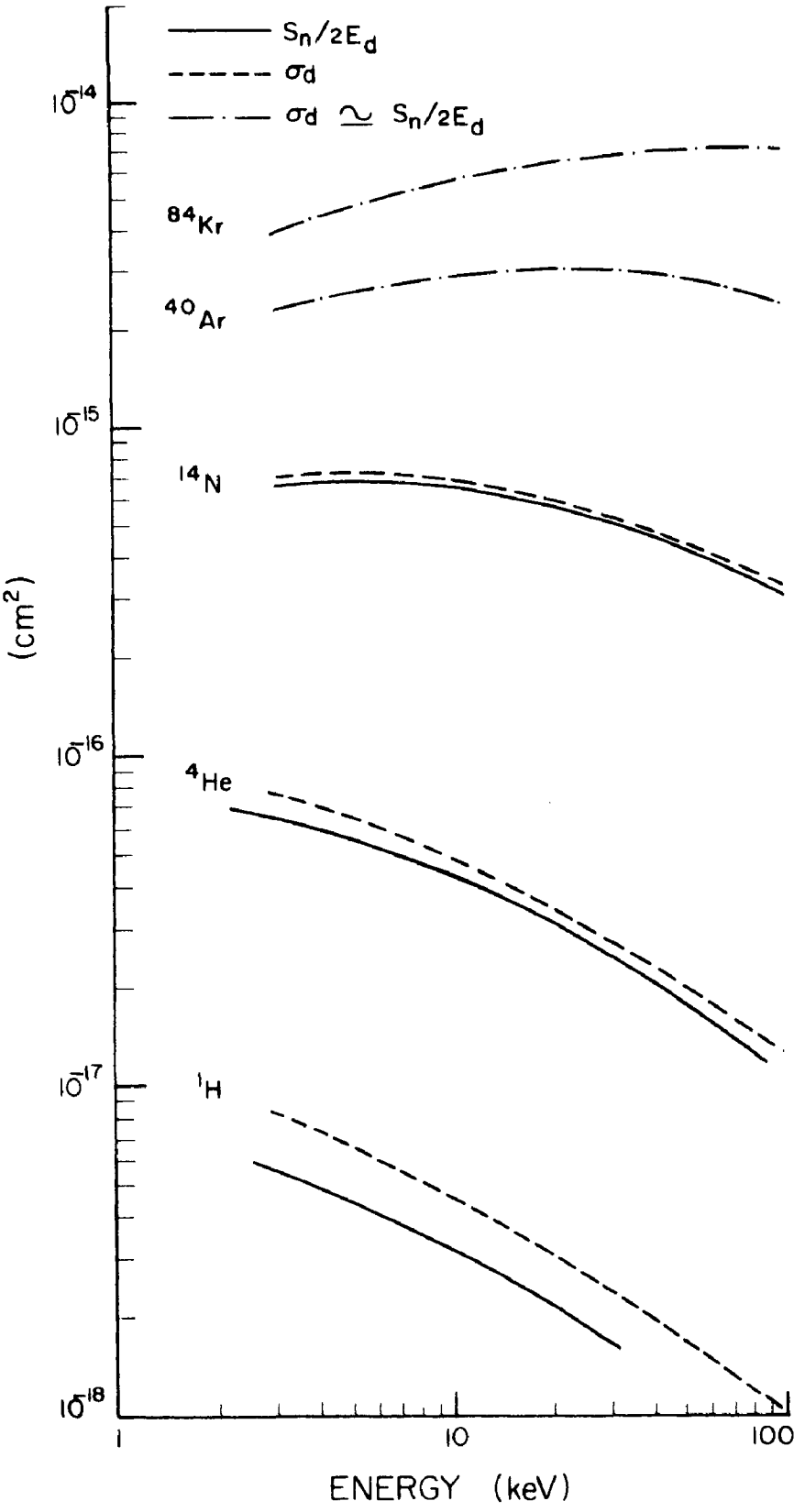

Fig. 29. A composite diagram showing logarithmic plots of S_n / $2E_d$ and σd both versus energy, for various projectiles in traversing a phypothetical (see text) medium with M_2=42 a. m. u. Z_2= 19.

REFERENCES

Beeler, J. R. and Besco, D. G., 1963. Conference J. Phys. Soc. Japan. 18 Supplement III, 159.

Broser, I. and Warminsky, R., 1951. Z. Natur. Forsch. 6a, 85.

Brown, F., Ball, G. C., Channing, D. A., Howe, L. M., Pringle, J. D. S. and Whitton, J. L., 1965. J. Nucl. Inst. and Meth., 38, 249.

Davies, J. A., Eriksson, L. and Jespersgaard, P., 1965. J. Nucl. Inst. and Meth. 38, 245.

Domeij, B., Brown, F., Davies, J. A. and McCargo, M., 1964. Can. J. Phys. 42, 1624.

Duckworth, H. E., 1958. Mass Spectroscopy, (Cambridge University Press) 34.

Eve, C. F. and Duckworth, H. E., 1958. Can. J. Phys. 36, 104.

Fastrup, B., Hvelplund, P. and Sautter, C. A., 1966. Kgl. Danske Videnskab. Selskab Mat. Fys. Medd. 35, 10.

Felder, R. M. and Kostin, M. D. 1966, J. Appl. Phys. 37, 791.

Hanle, W. and Rau, K. H. 1952. Z. Physik 133, 297.

Hastings, L. Ryall, P. R., and van Wijngaarden, A. 1967. Can. J. Phys. 45, 2333.

Heiland, G., Mollwo, E. and Stockman, F. 1959 Solid State Physics 8, 191.

Holmes, D. K., In Radiation Damage Nei Solidi, Edited by D. S. Billington (Academic Press, New York and London 1962), P. 182.

Kostin, M. D. 1966, J. Appl. Phys. 37 , 3801.

Lindhard, J. and Scharff, M. 1961. Phys. Rev. 124, 128.

Lindhard, J. Nielsen, V., Scharff, M. and Thomson, P. V. 1963a, Kgl. Danske Videnskab. Selskab Mat. Fys. Medd. 33 , 10.

Lindhard, J., Scharff, M., and Schiott, H. E. 1963b, Kgl. Danske. Videnskab. Selskab, Mat. Fys. Medd. 33, 14.

Lindhard, J. and Winter, A. 1964. Kgl. Danske Videnskab Selskab Mat. Fys. Medd. 34, 4.

Lutz, H., Schuckert, R. and Sizmann, R. 1965. J. Nucl. Inst. and Meth. 38, 241.

MacDonald, J. R., Ormrod, J. H. and Duckworth, H. E. 1966. Zeitsch. F. Naturf. 21a, 130.

McCargo, M., Davies, J. A. and Brown, F. 1963. Can. J. Phys. 41, 1231.

Ormrod J. H., MacDonald, J. R. and Duckworth, H. E. 1965. Can. J. Phys. 43, 275.

Robinson, M. T., 1965, Phil. Mag. 12, 741.

Sidenius, G. 1963. Atomic Collision Processes, Ed. McDowell, M. R. C. (North Holland Publishing Co), 709.

van Wijngaarden, A. and Duckworth, H. E. 1962. Can. J. Phys. 40, 1749.

van Wijngaarden, A., Bradley, D. J. and Finney, N. M. A. 1965. Can. J. Phys. 43, 2180.

van Wijngaarden, A. and Hastings, L. 1967. Can. J. Phys. 45,2239.

Young, J. R., 1955, J. Appl. Phys. 26 1302.

VITA

The author was born in Windsor Ontario on the seventh of March 1942. At the age of five he moved with his family to Amherstburg where he obtained his primary and secondary education. In 1959 he entered the University of Windsor (then Assumption University of Windsor) and received his Bachelor of Science degree in Physics in 1963, and his Master of Science degree in 1965.